TECHNICKÁ UNIVERZITA V LIBERCI
Fakulta strojní

Material response on the cavitation bubble collapses

Diplomová práce

Studijní program: N2301 – Mechanical Engineering
Studijní obor: 2302T010 – Machines and Equipment Design

Autor práce: **Edmund Ofei Aidoo**
Vedoucí práce: Ing. Miloš Müller, Ph.D.

Liberec 2018

TECHNICAL UNIVERSITY OF LIBEREC
Faculty of Mechanical Engineering

Material response on the cavitation bubble collapses

Master thesis

Study programme: N2301 – Mechanical Engineering
Study branch: 2302T010 – Machines and Equipment Design

Author: **Edmund Ofei Aidoo**
Supervisor: Ing. Miloš Müller, Ph.D.

Liberec 2018

Technical University of Liberec
Faculty of Mechanical Engineering
Academic year: **2017/2018**

DIPLOMA THESIS ASSIGNMENT

(PROJECT, ART WORK, ART PERFORMANCE)

First name and surname:	**Edmund Ofei Aidoo**
Study program:	**N2301 Mechanical Engineering**
Identification number:	**S16000271**
Specialization:	**Machines and Equipment Design**
Topic name:	**Material response on the cavitation bubble collapses**
Assigning department:	**Department of Power Engineering Equipment**

Rules for elaboration:

1. Research on the cavitation bubble-wall interaction.
2. Material properties at the impact conditions.
3. Design of experiment for the investigation of the material response on the cavitation impact.
4. Realisation of experiments with different cavitation or bubble intensity.
5. Results evaluation.
6. Results discussion.

Scope of graphic works:	**10 pages**
Scope of work report (scope of dissertation):	**50 pages**
Form of dissertation elaboration:	**printed**
Language of dissertation elaboration:	**English**

List of specialized literature:

[1] **Kim, K.-H., Chahine, G., Franc, J.-P., Karimi, A. (Eds.),** *Advanced experimental and numerical techniques for cavitation erosion prediction.* **New York, Springer, 2013. ISBN 9789401785389.**

[2] **FRANC, Jean-Pierre. a Jean-Marie MICHEL,** *Fundamentals of cavitation.* **Boston: Kluwer Academic Publishers, c2004. ISBN 1402022328.**

Tutor for dissertation:	**Ing. Miloš Müller, Ph.D.** Department of Power Engineering Equipment
Date of dissertation assignment:	**1 February 2018**
Date of dissertation submission:	**1 August 2019**

prof. Dr. Ing. Petr Lenfeld
Dean

L.S.

doc. Ing. Václav Dvořák, Ph.D.
Head of Department

Liberec, dated: 28 February 2018

Declaration

I hereby certify that I have been informed that Act 121/2000, the Copyright Act of the Czech Republic, namely Section 60, Schoolwork, applies to my master thesis in full scope. I acknowledge that the Technical University of Liberec (TUL) does not infringe my copyrights by using my master thesis for TUL's internal purposes. I am aware of my obligation to inform TUL on having used or licensed to use my master thesis in which event TUL may require compensation of costs incurred in creating the work at up to their actual amount. I have written my master thesis myself using literature listed therein and consulting it with my supervisor and my tutor. I hereby also declare that the hard copy of my master thesis is identical with its electronic form as saved at the IS STAG portal.

Date: 21/05/2018

Signature:

“Be strong when you are weak, brave when you are scared, and humble when you are victorious”

Michelle Moschetti

Abstract

Research on cavitation bubble-wall interaction and its impact on material properties has been discussed. The experiment was designed and realized with pitting test carried out during the incubation period on an aluminum alloy in a modified vibratory cavitation device. The amplitude of the device was kept at constant maximum and the polished surface of the sample was exposed to cavitation pressure pulses. The test was conducted at three different exposure times to ascertain the effect of exposure time on pit formation. The surface was analyzed using a Scanning Electron Microscope and a contact profilometer. The selection of appropriate cutoff depth for the analysis of the pits was discussed as well as the correction of the signal from the surface profile. These techniques allowed us to characterize the parameters of the pits such as diameter, depth, volume and pit numbers. The frequency distribution of the pit diameters was analyzed for both the SEM images and the surface profile of the profilometer. The effect of the exposure time on the distribution of pits was analyzed. It was determined that the exposure time significantly affects the number of pits formed as well as the distribution of pit diameters. The relationship between pit volume and diameter was analyzed. The distribution of pit volumes by pitting rate for different exposure times were also discussed. The surface deformation (pit depth) is seen to increase with increasing impact forces. The jet diameter, however, does not determine the extent of deformation since this phenomenon depends on other variables such as material properties, test conditions, and the magnitude of the impact force. The discussion given at the end attempts to explain the observations made in the study.

Keywords: Cavitation, Exposure time, Pitting rate, Material response

Acknowledgments

I am grateful to God Almighty for the gift of life and wish to dedicate this work to the memory of my late mother Joyce Ofei. I wish to thank Abena Acheampong for taking care of me for the most part of my life and for her unwavering support in my quest to achieve success in life. I am grateful to my supervisor Ing. Milos Muller, Ph.D. who has been immensely supportive and guided me through this work. A very big thank you to Ing. Jan Hujer who has been the backbone for the success of this project. I am grateful for your advice and taking time off your busy schedule to assist me. I wish to extend my gratitude to the Ministries of Youth and Sport for the Czech Republic for awarding me a government scholarship. I hope I can pay back your kindness in the very near future. My gratitude goes to Ing. Totka Bakalova, Ph.D. for supplying me with the profilometry measurements for my experiment. Additionally, I wish to thank Ing. Adam Hotař, Ph.D. for assisting with the initial Electron Microscopy measurements and a very big thank you to Ing. Pavel Kejzlar, Ph.D. for assisting with the Scanning Electron Microscope images. To Dr. Bernard Asimeng, I say a very big thank you for being supportive and believing in me. To all those whose names I cannot list here, I want to you to know that I remember how much you have helped me in getting here. I will forever be indebted to you for your kindness.

This study was supported as part of the project (SGS no. 21182) "The cavitation phenomenon and its erosion potential" with the support of the Specific University Research Grant.

Table of Contents

List of Symbols and Units

Symbol	Description	Unit
R	Bubble radius	$[m]$
$R(t)$	Bubble radius as a function of time	$[m]$
$\dot{R}$	First order derivative of bubble radius	$[m/s]$
$\ddot{R}$	Second order derivative of bubble radius	$[m/s^2]$
R_0	Initial bubble radius	$[m]$
$p(R)$	Boundary pressure	$[Pa]$
p_v	Vapor pressure of the liquid	$[Pa]$
p_∞	liquid pressure at an infinite distance from the bubble	$[Pa]$
p_i	Pressure inside the bubble	$[Pa]$
ρ	Density of the liquid	$[kg/m^3]$
r	Distance from the center	$[m]$
t	Time	$[s]$
$u(r,t)$	Simultaneous velocity at a distance r from the center	$[m/s]$
$p(r,t)$	Pressure of the liquid at a known distance r and time	$[Pa]$
p_{min}	Minimum pressure of the flow field	$[Pa]$
σ	Surface tension coefficient	$[N/m]$
μ	Liquid viscosity	$[Pa\ s]$
p_c	Critical pressure	$[Pa]$
V	Pit total volume	$[m^3]$
H	Pit depth	$[m]$
V_d	Volume damage rate	$[m^3/s]$
P_{jet}	Upstream pressure	$[Pa]$
P_{tank}	Downstream pressure	$[Pa]$
σ_{jet}	Cavitation number of jet	[-]
s	Standoff distance	$[m]$

List of Figures

List of Abbreviations

SEM	Scanning Electron Microscope
3D	Three dimension
LED	Light Emitting Diode
ASTM	American Society for Testing and Materials
KHz	Kilohertz

1.0 Research on Cavitation Bubble Wall interaction

This chapter introduces the general concept of cavitation and bubble dynamics. The concept has been classified and the general effects of cavitation have been outlined. The mechanism for bubble collapse close to solid boundaries and the general description of bubble collapse patterns have been discussed.

1.1 Introduction

A distinguishing feature which describes the hydrodynamic behavior of liquids is the ability for a two-phase vapor–gas flow to coexist [1, 2]. This unique phenomenon is known as cavitating flow. The physio-chemical properties of the liquid in addition to the hydrodynamic behavior can be significantly altered affecting flow conditions. As cavitation bubbles appear, submerged bodies may suffer from severe drag forces while moving through the liquid [3, 4]. In practice, however, cavitation bubbles have also found some useful applications such as in biomedicine, ultrasonic cleansing and many others [5–9]. Cavitation is not only limited to hydrodynamic flow but can occur in nearly static flow if the surface of the liquid is subjected to an oscillating pressure field that is large enough [10].

Cavitation is simply defined as the formation and dynamics of bubbles/cavities in a liquid medium. Cavitation can be characterized based on various phenomena such as surface tension, heat and mass transfer, nuclei content, viscosity and boundary layers [5]. The flow conditions and physical properties of the liquid affect the onset and propagations of cavitation bubbles. At the inception of cavitation bubbles, tiny voids or nuclei may appear in an initially homogeneous liquid medium. If the nuclei form as a result of the intermolecular interaction, the effect is known as homogeneous nucleation. In cases where the cavities are formed by the interaction of the molecules with the surrounding wall, such cavities are described to be heterogeneously nucleated. The cavities may then be filled with vapor, gas and in some cases even remain void. The interactions of bubbles with each other lead to the expansion of preexisting cavities to sizes where the macroscopic effects such as acoustic emissions and erosive properties can be observed. This process is dependent on

the flow parameters as well as the physical properties of the liquid. At the microscale, cavitation is also expected to significantly influence the design of high-speed microfluidic systems [11].

1.2 Classification

Cavitation can be classified based on the dynamic state of the liquid. For a liquid that is in dynamic motion along narrow passages, Venturi nozzles or in a pump, the pressure of the liquid decreases as a result of the sudden acceleration of the liquid. If the pressure of the liquid falls below the vapor pressure of the liquid (see *Figure 1*), the liquid may vaporize and cause cavitation to occur. Cavitation in flowing liquids is termed as *hydrodynamic* cavitation. Cavitation is however not limited to flowing liquids. In a nearly static liquid, the rapid acceleration of a solid body with sharp edges can create cavitation bubbles. The growth of preexisting microbubbles under the influence of ultrasonic field is also termed as *acoustic* cavitation and occurs under the free surface of the liquid.

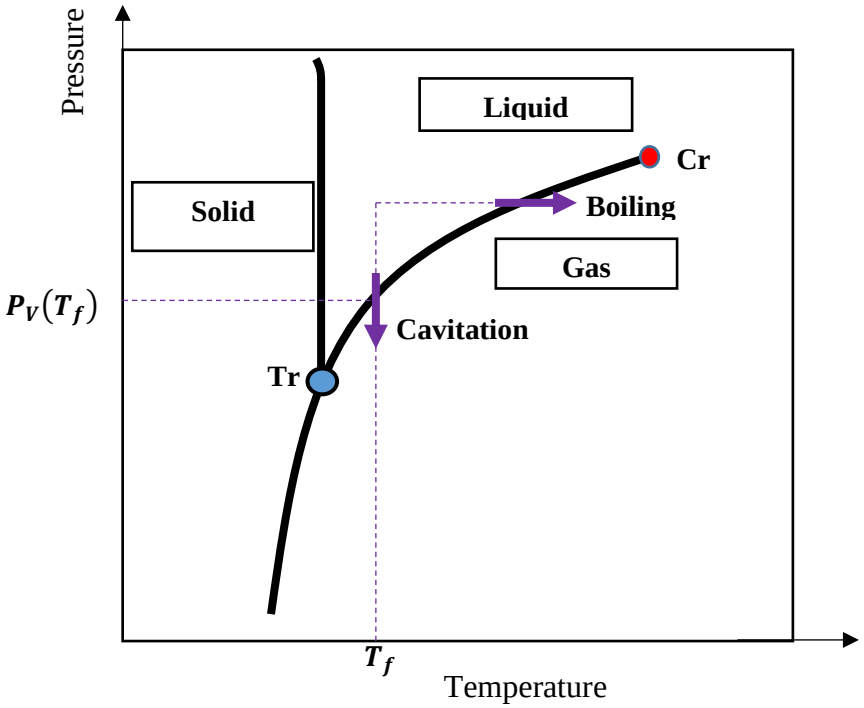

Figure 1: Phase diagram of water depicting cavitation and boiling

Another way of classifying cavitation is based on the bubble content. Through the process of mass diffusion across the boundary of the bubble, or reducing the pressure of the liquid, gas-filled bubbles can be made to undergo cavitation by keeping the liquid at a nearly constant temperature. For a vapor filled cavity, the ambient pressure of the liquid can be kept constant while increasing the temperature of the liquid above the saturation temperature. The vapor-filled bubbles have been divided into two forms. Firstly, a subcooled liquid case in which the latent heat is assumed to have no effect on the motion of the liquid because of the liquid's low density. Here, the motion of the liquid depends on its inertia [12]. The second case involves a superheated liquid. This process of superheating the liquid causes a rather explosive vaporization inside the cavity and depends on pressure changes as well as the control of the flow dynamics [13]. The effect is similar to boiling but the vapor-bubble dynamics in the boiling process depends on latent heat flow rather by the liquid's inertia [14].

Cavities that are predominately filled by vapor tend to take several forms after cavitation inception. The initial non-cavitating flow structures control the cavitation start process but as it develops further, the vapor structures tend to modify the flow properties causing the cavitation bubbles to take many forms. The flow velocity for instance increases when the rate of supply of the cavitation bubbles in the erosion region increases and results in increased impulsive pressure pulses induced by the collapsing bubbles. There are three main identified patterns that the cavitation bubbles can be grouped into. Transient isolated bubbles appear around low-pressure sides of the flow implode when they encounter area with high adverse pressures. They are influenced mainly by the air content of the liquid and are known to exhibit relatively weak erosive properties. On the low-pressure sides of blades and foils, cavitation bubbles can take the form of micro-cavities when a solid body which acts as a wall is placed in the flow. While this flow is very common, the hydrodynamic conditions result in a cavitating flow that shows different complex regimes. One of such regimes is the sheet cavitation which is normally characterized by thin, smooth and stable cavities. Another example is cloud cavitation which exhibits highly unstable turbulence and has high erosive properties capable of inducing abnormal dynamic behavior of turbomachines. These two regimes described are examples of attached or sheet cavities. The third type is known as cavitating vortices which occurs when the low pressures generated in a flow with concentrated vorticity can result in cavitation in the cores of the vortices and they exhibit their erosive strength once the tips of the vapor filled vortices are in contact with a solid wall.

1.3 Effects of Cavitation

Hydraulic systems are typically designed to operate in a homogeneous liquid. The impact of cavitation on these systems produces undesirable effects which greatly alter their performance and reduces efficiency. The formation of vapor structures in the liquid medium creates unstable regions in the flow and as a result, causes the pressure to reduce leading to a bubble collapse. There are three main undesirable effects that are caused by cavitation: (i) head losses, (ii) damages resulting from pit formation and eventual erosion of the solid body, and (iii) noise and vibration caused by the structural damage [15]. It is important that the impact of cavitation on a structure must be taken into account when designing hydraulic systems in order to have the equipment performing at their highest efficiency.

While most designers are faced with the dilemma of avoiding cavitation altogether, it has found several uses in other areas. In biomedicine, acoustic cavitation has been used for localized drug delivery. Cavitation also may be able to induce sonoporation, a transient cell permeabilization process that can allow nonviral gene transfer to a particular localized target on a tissue volume [16]. The ultrasonic agitation has been used to generate cavitation to improve the cathodic current efficiency of copper electrodeposited from dilute acidic sulfate. This approach allows the easy recovery of metals from waste solutions and helps to recycle the acids and bases in the solution [17].

1.4 Dynamics of Cavitation Bubble

The destructive action of cavitation bubbles in liquids has sparked numerous research in order to understand its dynamics [18–24]. According to Blake and Gibson [12], cavitation inception normally occurs downstream from the point of minimum pressure just prior to the separation point causing the bubbles to be swept up over the separation bubble. The reattachment of the separated flow shows regions where structural damages seem to occur. Earlier works involving spherical bubbles include Rayleigh [25] who solved the cavitation erosion caused by a spherical cavity in an infinite medium under uniform pressure at infinity for a non-viscous liquid. Knapp [26]

discovered that the physical properties of the liquid and the velocity of flow significantly affected the intensity of the cavitation bubble impacts on the cavitating regions. Lauterborn and Bolle [27] reported on cavitation bubble velocities plotted as a shape-time diagram and compared the shape-time dependence calculated by Plesset and Chapman [28]. Their findings were in agreement, supporting the implosion mechanism of cavitation by Rayleigh stating that the pressure pulses produced by the collapse of the bubbles resulted in damage to the walls [12]. The laser-induced cavitation bubble produced by Lauterborn and Bolle [27] also allowed feasible complex studies of cavitation bubble collapses under extremely highly controlled conditions free from mechanical destructions.

In order to describe the dynamics of the bubble, it is assumed that the effects of surface tension and liquid viscosity are neglected and the liquid considered as incompressible. It is also important to understand the evolution of pressure and velocity as a function of time. Rayleigh [29] showed from the momentum equation that the bubble boundary $R(t)$ obeyed the relation;

$$R\ddot{R} + \frac{3}{2}\left(\dot{R}^2\right) = \frac{p(R) - p_\infty}{\rho} \tag{1}$$

Where p_∞ is the pressure of the liquid at an infinite distance from the bubble, ρ is the density of the liquid, $p(R)$ is the boundary pressure. Rayleigh also assumed that the pressure at the center of the bubble to be same as the pressure of at the boundary. The relation that describes the incompressibility of the liquid velocity at a distance r from the center is given by

$$u(r,t) = \frac{R^2}{r^2}\dot{R} \tag{2}$$

Using the Bernoulli equation, the pressure in the liquid is found to be

$$p(r,t) = p_\infty + \frac{R}{r}[p(R) - p_\infty] + \frac{1}{2}\rho\frac{R}{r}\dot{R}^2\left[1 - \left(\frac{R}{r}\right)^2\right] \tag{3}$$

For a spherical bubble, viscosity affects only the boundary condition, therefore, giving us

$$p(R) = p_i - \frac{2\sigma}{R} - \frac{4\mu}{R}\dot{R} \tag{4}$$

Where p_i is the pressure inside the bubble, $p(R)$ the boundary pressure of the liquid, σ the surface tension coefficient, and μ, the liquid viscosity. The experimental observations on the cavitation-bubble growth and collapse can be described using equation (1) by considering p_∞ as a function of time [29]. Using equation (4), a generalized Rayleigh equation for bubble dynamics may be written as

$$R\ddot{R} + \frac{3}{2}\left(\dot{R}\right)^2 = \frac{1}{\rho}\left\{p_i - p_\infty - \frac{2\sigma}{R} - \frac{4\mu}{R}\dot{R}\right\} \tag{5}$$

The Raleigh-Plesset equation presents a way to temporally observe the evolution of the bubble radius and the influence of the pressure field inside the bubble, given that, p_∞ as a function of time is known. The equation can also be used to describe the bubble dynamics for an inviscid flow given that;

$$R\ddot{R} + \frac{3}{2}\dot{R}^2 = \frac{1}{\rho}\left\{p_i - p_\infty - \frac{2\sigma}{R}\right\} \tag{6}$$

For a given p_i and p_∞ where both are functions of time, an equilibrium bubble radius may be defined as

$$R_0 = \frac{2\sigma}{p_i - p_\infty} \tag{7}$$

If the effects of surface tension, non-condensable gas and viscosity are ignored, the bubble remains in an equilibrium before the initial time. It is realized that at the initial time where *t=0*, a constant p_∞ which is higher than p_v is applied to the liquid which results in the collapse of the bubble at a characteristic time τ known as the Rayleigh time. The evolution of the bubble at the end of the collapse is also described in equation (8).

$$\frac{R}{R_0} \cong 1.87 \left[\frac{\tau - t}{\tau}\right]^{\frac{2}{5}} \quad (8)$$

The Rayleigh model is good for the analysis of bubble dynamics for short duration and rapid change in its timescale. The global features of the first bubble collapse for an inviscid flow can be described using this model. However, it does not account for the successive collapses that are actually observed in real situations.

1.5 Bubble Collapse Near Rigid Walls

In *Figure 2* below, it is observed that reducing the minimum pressure, p_{min}, of the flow field below the critical pressure, p_c, of the bubble causes the bubble to grow explosively (in red) to a maximum size helping it acquire significantly high potential energy [30]. The blue line in *Figure 2* indicates little to no change in radius size if the minimum pressure p_{min} is kept above the critical pressure, p_c. At the maximum bubble size, the pressure inside the bubble reduces to a value close to the vapor pressure and results in a large pressure gradient with the liquid pressure.

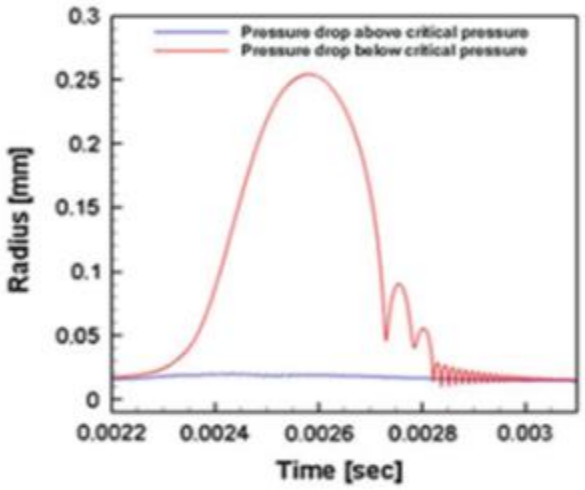

Figure 2: Bubble radius versus time in a propeller flow field [30]

Close bubble-boundary interaction induces a deformation in the cavity as a result of the anisotropy of the liquid particles motion during the collapse [31]. The potential energy contained in the expanded bubble is converted to kinetic energy of the liquid jet and penetrates the bubble in the direction of the nearest wall. In an attempt to estimate the potential damage [32–34] caused by the bubble collapse, Philipp and Lauterborn [35] reported damages to occur when the initial bubble distance close to the solid wall is less than twice the bubbles radius. Upon impact to the wall, the closeness of the boundary results in a radial flow away from the jet axis. The still-contracting bubble collides with this radial flow resulting in a "splash effect" which moves away see (*Figure 3*) in the direction opposite to the motion of the microjet.

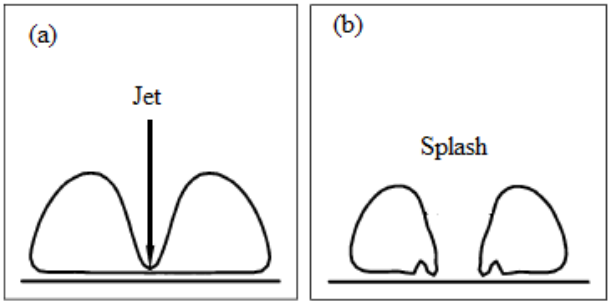

Figure 3: Bubble geometry (a) before, (b) after the impact of the reentrant jet on the opposite side of the wall [36]

The collapsing cavity also emits a shock wave which significantly contributes to the damages observed on solid walls. Shima *et al.* [37] reported shock waves to be seen in the re-expansion phase when a bubble collapses from a solid wall. The intensity of the shock waves increases when the bubbles collapse at a shorter distance to the solid wall. It is possible for the shock waves and jets to coexist. This usually occurs when a bubble touches the solid wall at its maximum expansion. Based on the contact angle to the wall, the impulsive force can be said to be contributed by the jet or the shock wave. Jet predominates the impulsive force when the angle of contact is acute to the wall and when this angle is obtuse, the impulsive force is said to be dominated by the shock waves.

1.6 Bubble Collapse Patterns

Müller *et al.* [34] investigated bubble collapse patterns at different distances to a solid wall using acoustical and optical methods. For bubbles that collapsed far from the solid, it was observed that the bubbles maintained a nearly spherical shape after collapse mainly due to the absence of microjets usually formed as a result of close wall-bubble interactions. Spherical bubbles generated much closer but not in contact with the wall revealed that as the bubble approaches the wall, the presence of the wall creates conditions that allow the anisotropy of the liquid to affect the bubble shape and dynamics. The bubble deforms and expands causing it to be accelerated towards the wall (*Figure 4*). The measured impact forces showed comparable values for the first and second collapses and the subsequent collapses, however, they had little impact magnitudes since most of the potential energy created by the expanding bubbles had been dissipated by the first two collapses. Patterns for bubbles collapsing very near to the solid wall showed the first expansion of the spherical bubble to be much smaller than the second collapse. The much-accelerated bubble rebounds of the wall after re-expansion with a distorted spherical shape and recorded a more intense impact force and pressure [38]. The significant increase in the magnitude of the second collapse is due to the effects of splashing.

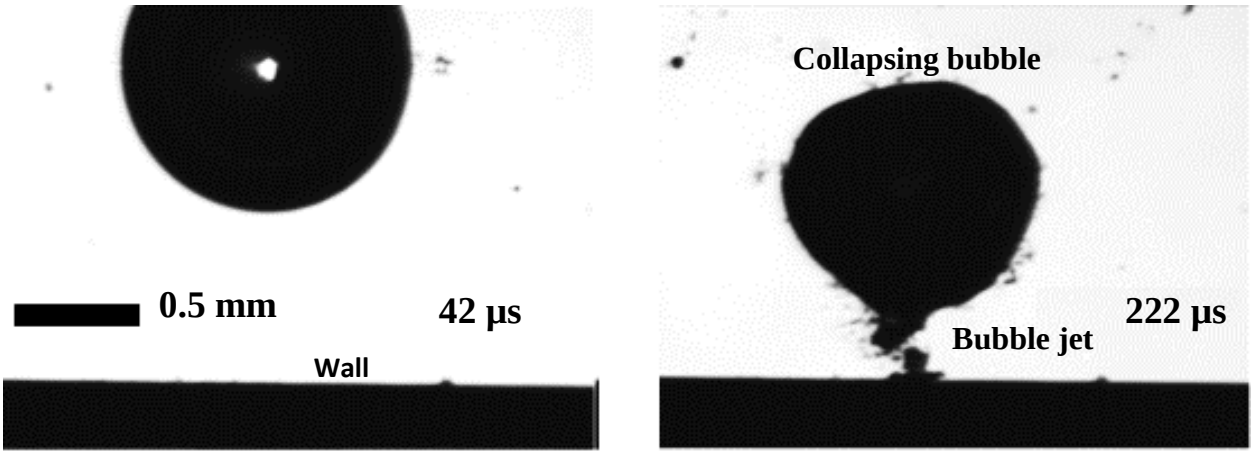

Figure 4: Collapsing bubble near solid wall [34]

1.7 Material Properties at The Impact Conditions

Structural deformations in materials are contributed mainly by elastic and plastic deformations. The stress-strain curve describes the effect of an increase in strain on stress (*Figure 5*). Stress is defined as load per unit cross-sectional area while strain is a measure of deformation that a stressed material experience. Any significant increase in strain will require a corresponding increase in stress to maintain same strain rate. Cavitation flow field is characterized by frequencies and amplitudes of high magnitudes with clearly mapped out pressure pulses which are known to produce bubbles that exhibit violent dynamic behavior such as explosive growth, collapse, and rebound. If a rigid body is placed within a cavitating flow field, it will experience repeated and randomly distributed impulsive loads (*Figure 6*a) that are independent of the loading mechanism (shockwaves, pressure waves or jets) [30]. If the magnitude of the load impacting the surface of the material is smaller than the critical mean stress of the material, the material will deform elastically. This deformation is not permanent and the material will return to its original form in time (*Figure 6*b). However local deformations may be formed on the materials exposed to cavitation as a result of short pressure pulses of sufficient magnitudes, usually greater than the critical stress of the material, are directed to the solid walls. This induces plastic deformations and leads to pit formations (*Figure 6*c). Over a period, a localized accumulation of these deformations cause material failure and consequently, the bulk erosion of the material. Karimi *et al.* [39] reported that the localized and repeated effects of cavitation stresses which induce the plastic deformation of substructures and the work hardening at a point found under the eroded surface results from two effects. One is the instantaneous effect of single impacts which causes a severe deformation at high strain rate in the impacted region. The other is the accumulation effects of the multiple impacts exposure of the material to the cavitation flow field that gradually increases the internal hardening in deeper layers. Moreover, for spherical indentations, if the depth of the indenter is very small, the deformation caused by the indentation is seen to be dominated by the elastic hardening with little to no plastic deformations. Small depth indentations are constrained from exhibiting plastic deformations by the surrounding material undergoing elastic deformation. Indenters with much bigger depth cause large deformations dominated by extensive plastic hardening[40]. Thus, a careful consideration of the strain rate will provide a better understanding

of the erosion behavior of different materials as well as to elaborate more accurate predictive models for a long-term erosion.

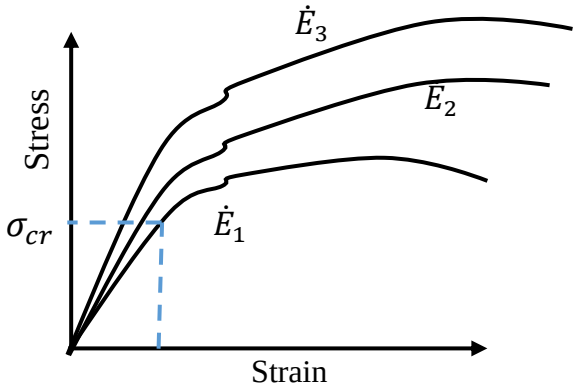

Figure 5: Stress-strain curve

(a) (b) (c)

Figure 6: (a) Material under stress, (b) recovery from elastic deformation, (c) plastic deformation

2.0 Laboratory Testing Methods

Machine design has undergone radical improvements to make sure that they function efficiently and last long. For any material designed to withstand cavitating flow fields, it is necessary to assess its performance on multiple tests to ensure that it does not suffer from the adverse effects of cavitation erosion. The tests may be carried out in small-scale laboratories or on an industrial scale. Two popular the techniques for evaluating material resistance to cavitation include the use of ultrasonic transducers (Vibratory Cavitation Device) and cavitating liquid jets and their use are in accordance with the ASTM G32 and ASTM G134 respectively.

2.1 Vibration Cavitation Apparatus

Cavitation here is generated by a vibratory device with components such as a generator, transducer, sonotrode (horn), a beaker filled with a test liquid (usually de-ionized water). The test specimen can be attached to the tip of the sonotrode or indirectly placed opposite to the tip of the sonotrode (see *Figure 7*). The vibratory motion of the sonotrode generates pressure waves directly against the surface of the test sample usually at a frequency of 20 KHz. The Intensity of the pressure waves affects the sample when the sample is directly affixed to the tip of the sonotrode. This has been reported to give different results compared to running the test with the surface of test sample placed at a certain distance (gap distance) away from the tip. Pola *et al*. [41] carried out cavitation erosion tests to observe the effectiveness of ultrasound treatment of liquid aluminum alloys in improving the mechanical properties of the materials. They concluded that the cavitation erosion treatment significantly improved the erosion resistance of the material by increasing the homogeneity of the microstructure. Additionally, Devi *et al*. [42] evaluated the performance of several materials at different testing conditions such material type, exposure time, gap distance, liquid characteristics, as using the vibratory device. They concluded that all of these variables significantly affect the resistance of the material to the cavitation erosion.

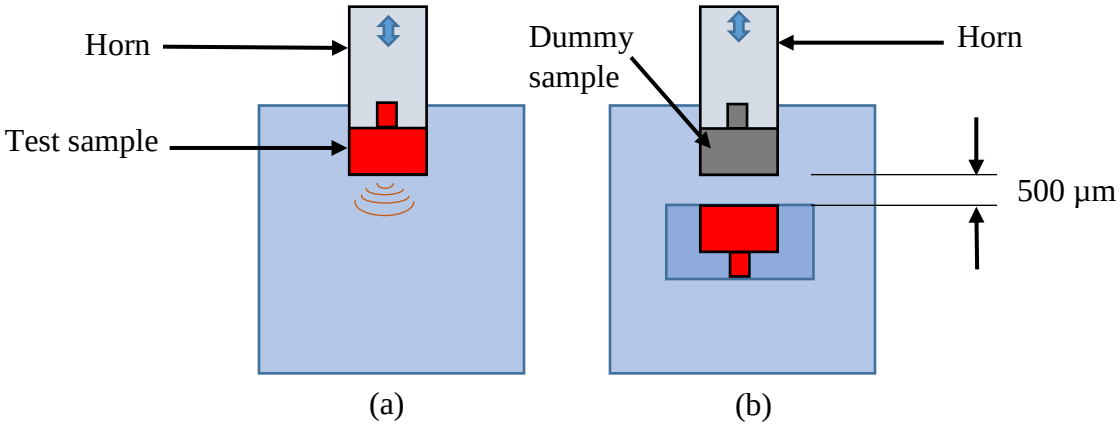

Figure 7: Vibratory cavitation apparatus (a) direct method, (b) indirect method

2.2 Cavitating Liquid Jets

The intensity of cavitation produced by jets can be altered by adjusting the jet velocity, angle, diameter and the liquid's ambient pressure. This added flexibility makes it a very useful technique for determining the effects of cavitation on material behavior [43–45]. This is particularly obvious when the realistic bubble clouds generated by the cavitating liquid jets is compared to the ultrasonic horn. It is well known that cavitation if controlled, can be used to improve material fatigue strength. Soyama *et al*. [46] successfully formed residual stresses by cavitating jets and used it to strengthen the surface of the test material. The test liquid passes through a tap hole into a nozzle with a throat diameter that can be controlled. A pump with a very high capacity is used to ensure that the nozzle can have a significantly high discharge rate. The pressure of the test liquid injected into the tap hole is recorded as an upstream pressure, P_{jet} and the downstream pressure, P_{tank} is defined as the pressure located within the test section. The distance from the upstream corner of the nozzle throat to the surface of the material is defined as the standoff distance, s. An exit tap hole is created to allow the test liquid leave. Both tap holes are covered by valve openings. The sample is mounted in a sample holder and its surface placed perpendicularly to the direction of the moving cavitating jets from the nozzle. Cavitation number is considered a very important parameter of cavitating jets since cavitation occurs at the region with increased flow and reduced pressure [46, 47]. The ratio of the flow velocity and the pressure near the cavitating region defines

the cavitation number. Flow velocities for nozzles and orifices are mainly influenced by upstream and downstream pressure differences. Equation (9) below defines cavitation number.

$$\sigma_{jet} = \frac{P_{tank} - P_v}{P_{jet} - P_{tank}} \cong \frac{P_{tank}}{P_{jet}} \ll 1 \qquad (9)$$

The simplification in equation (9) is done because of the relation $P_{jet} \gg P_{tank} \gg P_v$. The reduction in cavitation number reveals a developing cavitating region.

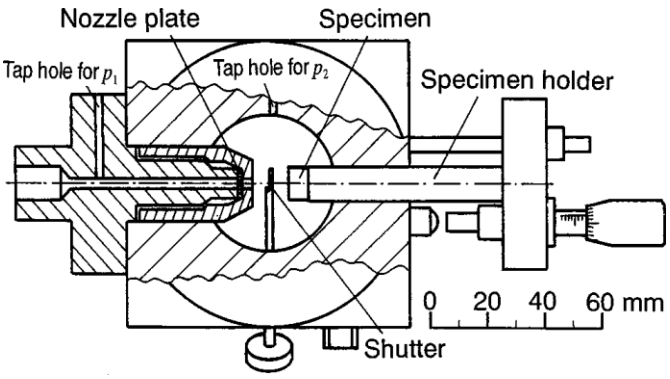

Figure 8: Test section of cavitation jet setup [46]

2.3 Methods for Evaluating Damaged Surfaces

Several methods have been evaluated in this section with a focus on the methods that are used for the extensive analysis of damaged surfaces of the materials.

2.3.1 Mass Loss Tests

The erosion behavior of cavitation pressure fields on a material surface depends on the properties of the material, and the conditions under which the erosion devices operate [47–49]. Cavitation erosion is therefore marked by different regimes and subsequently represented on a mass loss curve

of the material exposed to cavitation at a certain time. Cavitation damage depends on the intensity of the pressure field that impacts the solid boundary of the material [50, 51]. The incubation period marks the first stage of the regime. In this period, plastic deformation (described as pits) occurs on the exposed solid boundary. The material may experience microscopic deformation without any weight loss. The initial stage of the mass loss versus time curve shows a region where it is difficult to measure any mass loss. The duration of such resistance is an important parameter in determining the lifetime of most materials which shows any correlation between incubation time and material's lifetime [52].

The intensity of cavitation becomes greater as the exposure time increases. The formation of more pits leads to minute mass losses and modifies the boundary flow as the pressure field becomes heavily influenced [43]. This stage, known as the acceleration period results in severe changes to surface properties and behavior and it's followed by the deceleration period. The nature of this stage is marked by the dynamics of cavitation bubbles as a result of the changes to the material surface. The steady-state period shows an equilibrium between the erosive strength of the cavitation pressure field and material response. Mass loss measurements can be easily converted to volume loss to characterize the material response to cavitation erosion. The eroded profiles for several materials can be compared by setting different exposure times to determine the maximum erosion depth for the material since the materials have different resistance to cavitation erosion. The results of such tests show that the profiles are not same for all the materials even though the maximum erosion depth is set to a constant value and thus provides a means to an extent, to predict the long-term erosion behavior from short tests.

2.3.2 Pitting Test

The analysis of cavitation pits presents a way to estimate the extent of cavitation erosion damage and a model to understand how different materials respond to cavitation flow impacts. Several methods have already been used to evaluate cavitation erosion resistance. Pitting tests are usually carried out in short durations and offer a faster way to characterize the erosion resistance of a material as compared to mass loss tests. The major problems these tests face is that the laboratory results do not translate into the real world.

It is possible to obtain direct measurements of the cavitation bubble collapse using pressure transducers [53–57]. The development of other cutting-edge techniques has improved how the damaged surfaces are profiled. Example of such equipment includes the Optical Profilometer, Scanning Electron Microscope (SEM), and Laser Profilometer.

In an attempt to explain pitting formation, a pressure wave generated by a cavitation bubble was emitted at distance L towards the solid boundary (material's surface). After impact, the geometry of the pit (*Figure 9*) has a depth of H. The total pit volume (V) can be computed for the estimation of the volume damage rate.

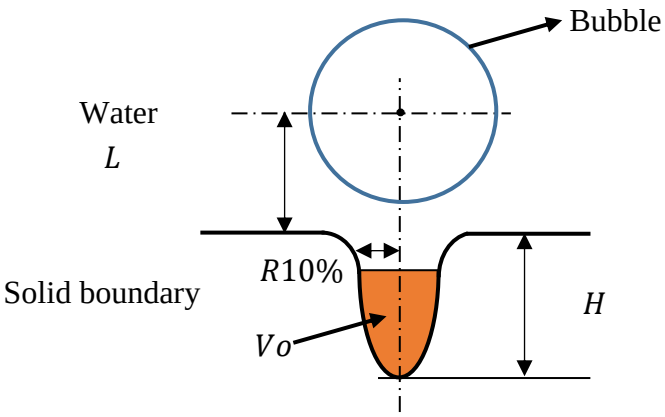

Figure 9: Profile of a pit

Carnelli *et al*. [58] evaluated the hydrodynamic peak of pressure distribution to measure stress and load distribution in a cavitation pit. They modeled the hydrodynamic impact loads distribution and also used data from nanoindentation measurements. Soyama *et al*. [57], proposed a prediction method of cavitation erosion rate using cavitation intensity of the cavitating jet and the material erosion rates. Fortes [59] attributed the formation of pit profiles by three main characteristic parameters which are: pit depth *H*, total pit volume *V*, and pit radius R_{cone}. The parameters are related by equation (10).

$$R_{cone} = \left(\frac{3V}{\pi H}\right)^{1/2} \tag{10}$$

The profile of the pit can then be represented by the equation

$$\frac{r}{R_{cone}} = f\left(\frac{h}{H}\right) \tag{11}$$

$$h = 0.1H \tag{12}$$

At a depth of h, the radius is calculated from the relation

$$\frac{R_{10\%}}{R_{cone}} = 0.9336 \tag{13}$$

The ratio between $R_{10\%}$ and H does not provide a constant value as it depends strongly on the characteristic wave pressure impact. This implies that another relation must be used in describing the characteristics of the pit profiles. The uncertainties result from the axisymmetric nature of the pits. From numerical tests, Patella *et al*.[60] deduced two parameters; total volume of the pit, and a reference volume.

$$V = 2\pi H R^2{}_{cone} \int_0^1 \frac{r'^2}{2} dh' \tag{14}$$

The values r'=r/R_{cone} and h'=h/H. The reference volume can then be calculated equation (15).

$$V_o = 2\pi H R^2{}_{cone} \int_{1/3}^1 \frac{r'^2}{2} dh' \tag{15}$$

The summary of the simulation results in the final approximation of the volume ratio for a non-dimensional pit profile in equation (16) below from the maximum pit depth H.

$$\frac{V}{V_o} = 4.9 \tag{16}$$

The reference volume V_o, can be calculated using some numerical software. The total pit volume V can then be calculated using equation (16). The values of V, R_{cone}, and $R_{10\%}$ can then be calculated from the equation (16,15,14 and 13) respectively. Using this approach provides a better approximation of experimental pit volumes because it is not affected by the uncertainties in measurements caused by surface oscillations.

2.3.3 Scanning Electron Microscope

Marques and da Exaltação Trevisan [61] reviewed the behavior of cavitation resistance of several materials and realized the difficulty in comparing test results obtained from the many cavitation tests available. The Scanning Electron Microscope (SEM) technique has been used to study test surfaces from cavitation providing an optical description so vivid in helping understand structural deformations at the microscopic level. The particle residue and the surface of the test sample can both be imaged by the SEM (*Figure 10*) and used to describe the extent of the damage. Fine residues often depict less damage and often little mass loss while a coarse residue in the SEM micrograph depicts a more extensive mass loss. The surface of the test sample can also reveal damages which cannot be easily seen with the naked eye. SEM Micrographs are however not ideal for describing plastic pits formed in the incubation period. They are also difficult to be geometrically characterized [62].

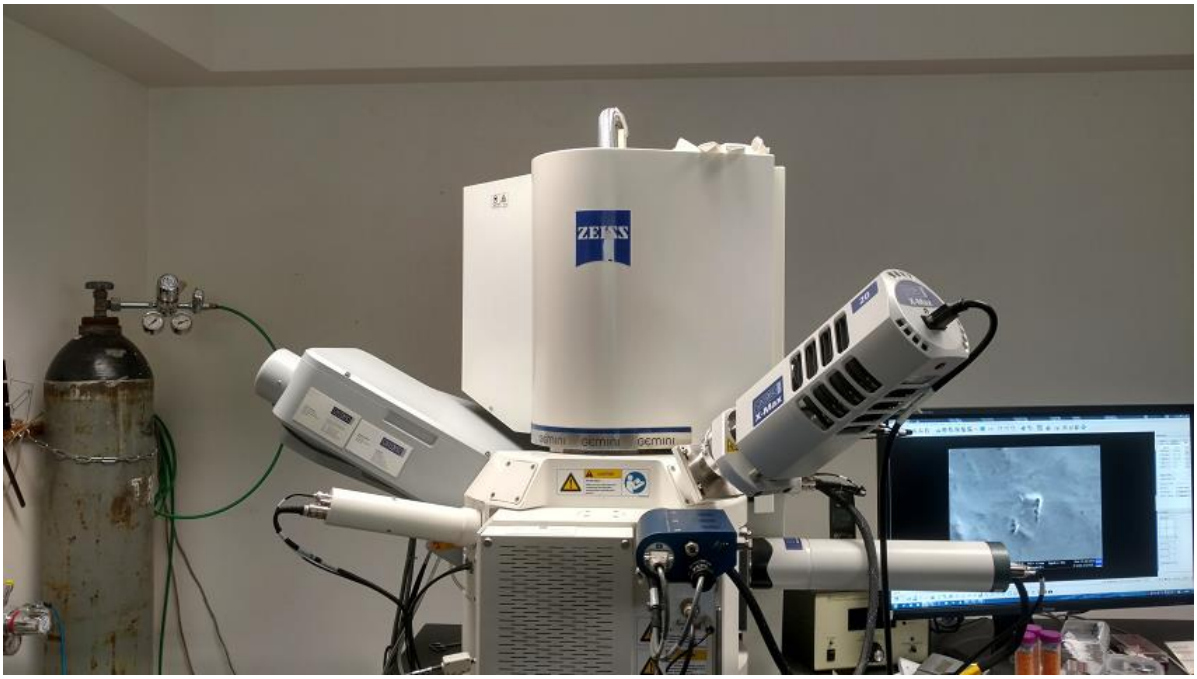

Figure 10: ZEISS GeminiSEM – Field Emission Scanning Electron Microscope

2.3.4 White Light Interferometer

The device consists of a beam splitter, a light emitting diode (LED) source, a camera and a reference place. The light from LED is split into two, a reference beam and a measurement beam by the beam splitter. The reference beam is reflected from the reference plane while the measurement beam is incident on the surface of the sample. Optical interference occurs at every point of the surface where the optical path length is the same as both the reference and measurement beams. The interference patterns are captured by the video camera while the topography is computed by a software using the data from the interference. This technique allows lateral resolutions of 9 µm to 50 µm to be measured. The 3D high precision profiler offers a non-destructive description of surface topography and gives information about the texture and roughness of the surface. Furthermore, this technique has shown close correlation with other results and has proven to be reliable [62].

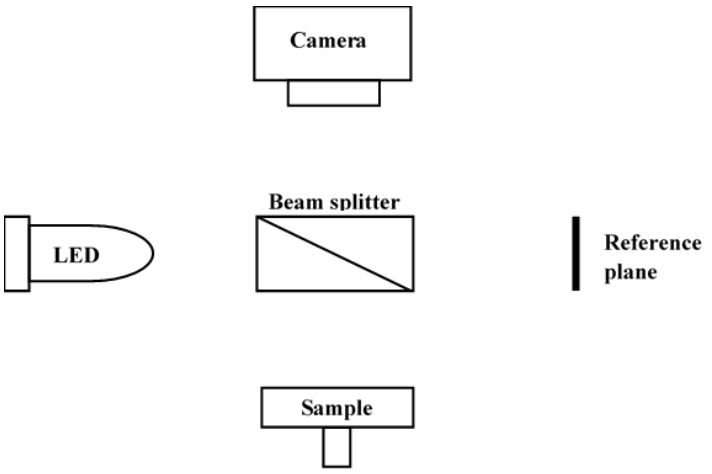

Figure 11: Schematic description of the white light interferometer

2.3.5 Surface Analysis in Software

To analyze the topographic data from the surface profile of the sample in Matlab, a mean depth over the entire image is established to allow the removal of undulations created by the Profilometer. This helps deal with the surface inclination problems. The mean depth is also the zero level that serves as a reference for the measurements of pit depth, diameter, and volume. By setting a threshold value, cavitation pits with depths and diameters greater than the set value can be identified and characterized. Matlab is used for the analysis and depending on the cutoff value set may take up to three (3) minutes for complete identification of the pits [63]. The results for pit diameter, depth and volume are exported for further analyses if required. 3DSM Metrology software can also be used for the thorough analysis of optical micrographs. The surface data can be used to detect individual pits parameters such as maximum diameter and area.

3.0 Experimental Design

This chapter describes the materials used for the experiment. The preparation methods used for the samples and the design of experimental setups for the measurement of cavitation bubbles have been discussed.

3.1 Materials

In this work, an aluminum alloy (EN AW-7075 T6511) was selected for testing. The nominal chemical composition and Mechanical properties are listed in Table 1.

Table 1 Chemical and Mechanical properties of the test sample

Chemical composition							
%							
Si	Fe	Cu	Mn	Mg	Cr	Zn	Ti
0.1	0.19 to 0.20	1.5	0.16	2.6	0.2	6.0	0.04
Mechanical Properties							
Tensile strength			Yield strength		Elongation		
[Mpa]			[Mpa]		[%]		
576			521		8.5		

3.3 Sample Preparation Methods

This section deals with the different methods used to prepare the sample for the experiment. It includes the dimensions used for the machining of the sample as well as the surface polishing techniques used.

3.3.1 Dimensioning

The alloy was machined according to the dimensions provided in (*Figure 12*).

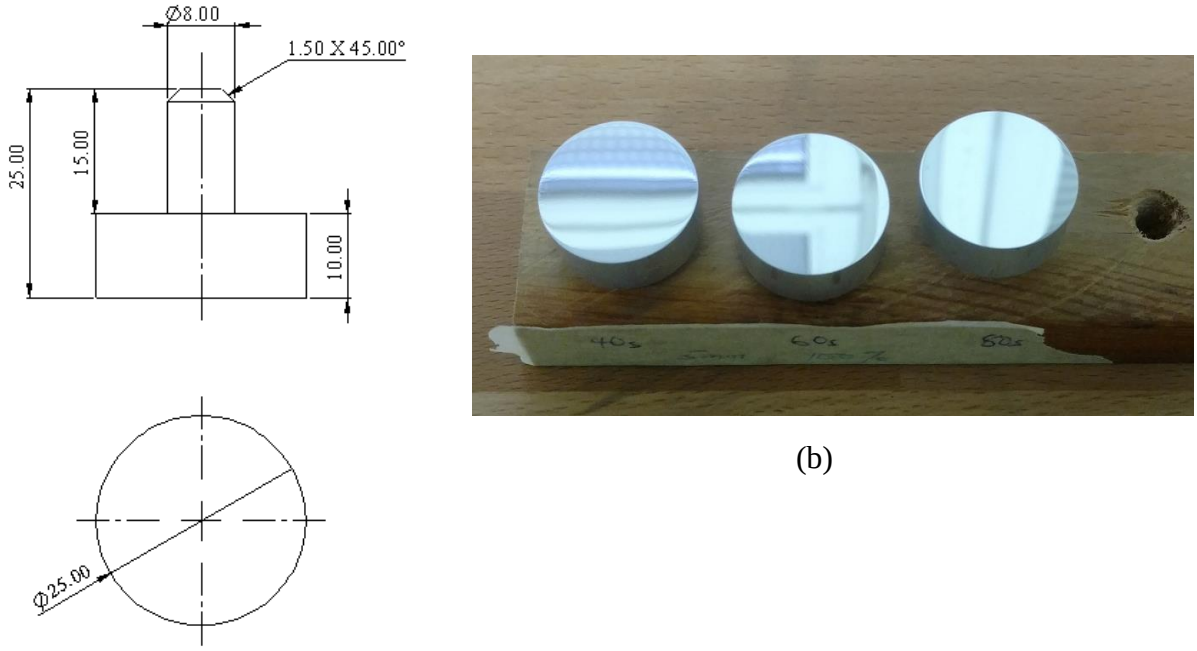

(a)

(b)

Figure 12: (a) Drawing of the test sample with dimensions, (b) Test sample placed in a sample holder

3.3.2 Grinding

The surface of the test sample was first prepared by grinding it on a sandpaper placed in the Buehler 2 speed grinder and then finely polished with the Buehler Metaserv 3000 variable speed grinder-polisher. Two sandpapers grits were used. The 600-grit sandpaper was first used. The surface was ground in one direction and then rotated about 90 degrees for further grinding. The speed of rotation of the machine was set first set to low and gradually increased to intermediate while tap water was intermittently run on the sandpaper to help reduce the effects of temperature increase while grinding. The sample was then cleaned and dried. The 600-grit sandpaper was replaced with the 1200-grit sandpaper and extra grinding. The higher grits deliver a smoother finish. The samples were then finally washed with water and sprayed with cleaning alcohol before drying under a hand dryer.

(a) (b)

Figure 13: (a) Buehler 2 speed grinder-polisher, (b) MetaServ® 3000 variable speed grinder-polisher

3.3.3 Polishing Techniques

In order deliver a mirror-like finish, the samples are polished with two different polishing cloths. The first is an intermediate TriDent 3μm diamond abrasive polishing cloth. The cloth spins in the grinding machine (*Figure 13*a) and a cleaning solution, MasterMet ^{TM} 2 (a non- crystallizing colloidal Silica polishing suspension) was applied to the cloth. In order not to transfer tiny particles (dirt) which could destroy the polishing cloth and subsequently the surface of the sample, the sample was cleaned after each stage with distilled water and sprayed with cleaning alcohol. The sample was then transferred to the grinder-polisher (*Figure 13*b) fitted with a fine ChemoMet 0.05 μm cloth. The samples were then gently packed into a holder for safe keeping. The sample holder was placed into a protective box to avoid accidentally scratching the surface by falling objects.

3.4 Selection of Optimal Gap Distance and Exposure Times for The Experiment

Preliminary tests were carried out in order to determine the optimum *gap distance* between the tip of the sonotrode and the sample as well as the *time* to *expose* the surface of the material to in order to create well-formed and easy to identify pits. It was determined that using a gap distance of 3mm

created pit clusters which make it difficult for characterizing the individual pits (see *Figure 14*). Thus, the intensity of the pits formation increased as the exposure tie also increased. Upon increasing the gap distance between the tip of the sonotrode and the surface of the sample, it was realized that the pits could be easily identified (see *Figure 15*). This has a huge potential in helping reduce the errors that could be associated with pit characterization. Additionally, exposing the surface of the samples to similar times in both cases allowed a careful observation of the effects of time and gap distance on the sample. A gap distance of $5mm$ and $40s$, $60s$, $80s$ exposure times were selected for conducting this experiment. The aim was to identify a significantly large number of pits (200 to 300) within the set threshold for characterization.

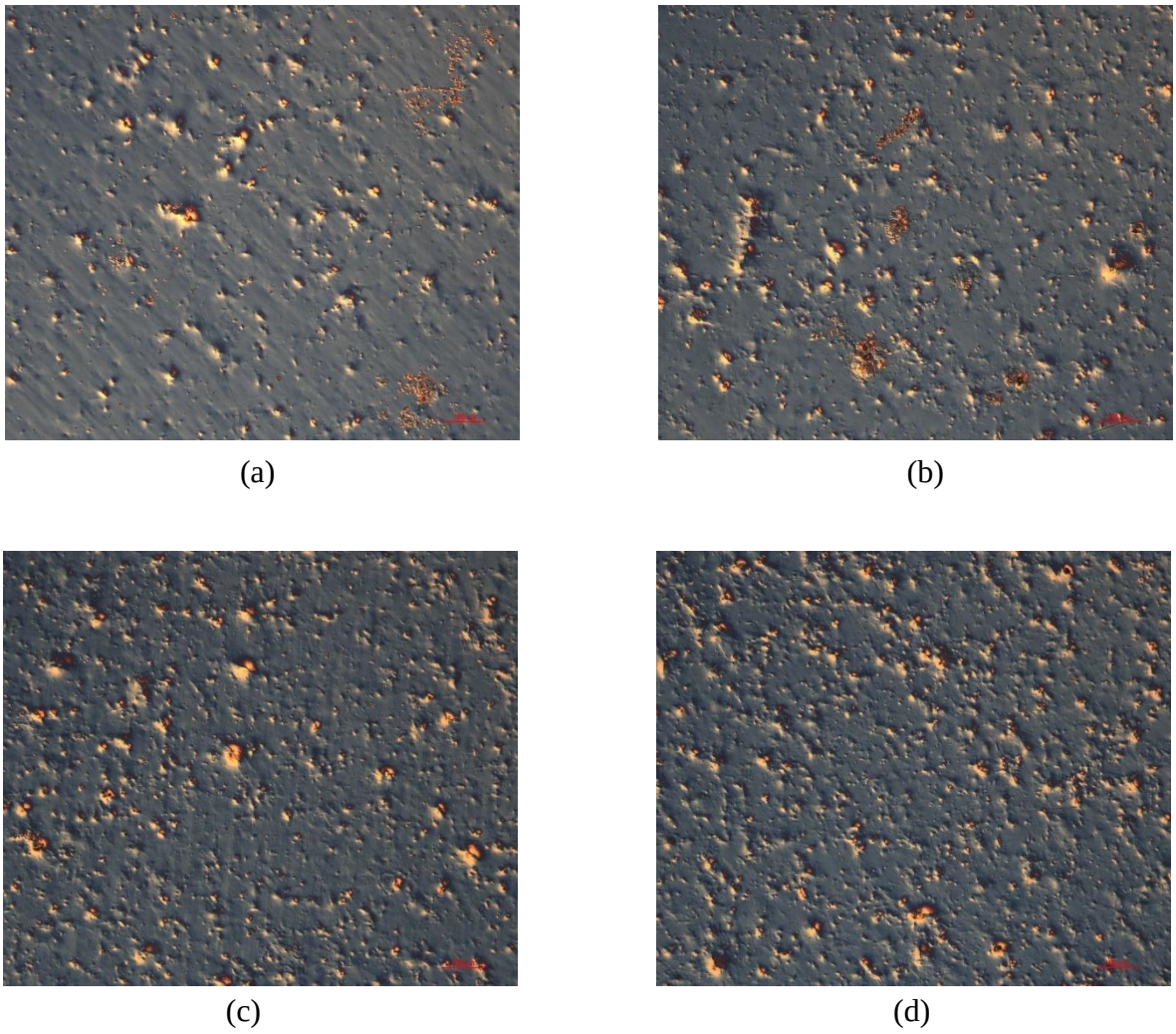

(a) (b)

(c) (d)

Figure 14: 100X magnified micrograph with 3mm gap obtained at times (a) 10 s, (b) 20 s, (c) 30 s, (d) 60 s from central position

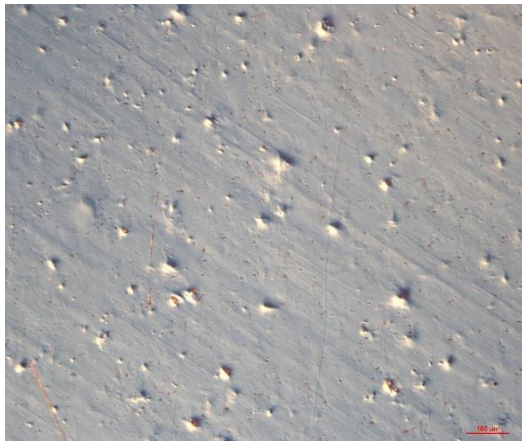

(a)

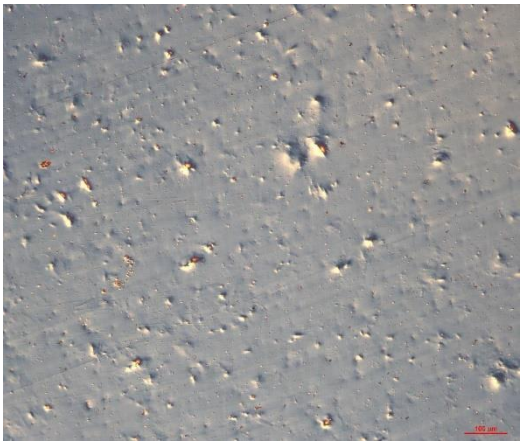

(b)

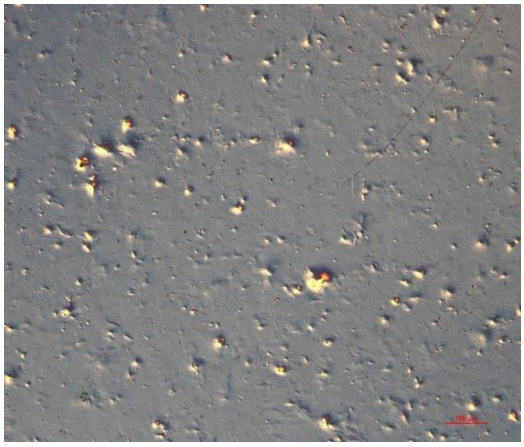

(c)

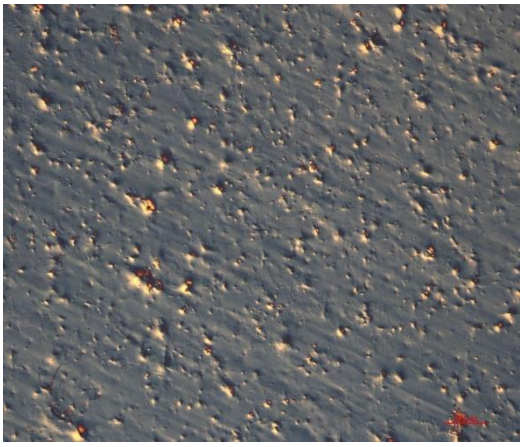

(d)

Figure 15: 100X magnified micrograph with 5mm gap obtained at times (a) 10 s, (b) 20 s, (c) 30 s, (d) 60 s from central position

3.4 Cavitation Erosion Test using a Modified ASTM G32 Vibratory Apparatus

A modified vibratory cavitation tester was used to conduct the test. The pitting test was carried out using the following recommended standards (see *Table 2*). This method offers a simple and controlled test and often allows cavitation erosion resistance of different materials to be compared. In the setup of this method, a velocity transformer or horn is attached to an ultrasonic transducer capable of generating up to 20-kHz frequency. The sample to be studied is initially cleaned with

alcohol spray and carefully dipped in a distilled water before being placed in the sample holder. The specimen is then fastened to test holder and held in place by three vertical rods that attach to the ultrasonic transducer by nuts and washers.

Table 2 Cavitation pitting test properties

Parameter	Value	Unit
Frequency of vibration	20±0.2	kHz
Vibration amplitude	57	μm
Gap between horn and sample	5	mm
Temperature of water in beaker	25±1	^{0}C

To ensure that the sample was kept at the recommended height (gap distance) below the sonotrode, a standard measurement gauge block was used. This was done carefully to avoid unnecessarily damaging the surface of the sample. A beaker was placed beneath the sample and filled with distilled water to the brim. The beaker was kept at the desired height by placing a support beneath it. Pitting usually forms in the incubation period of cavitation and therefore requires a minimum exposure time of the sample to the pressure waves generated by the transducer [64]. The transducer was set to operate at a controlled amplitude and frequency. The generator shown in (*Figure 16*c) was turned on while a timer was set to monitor the exposure time to the cavitation bubbles. In this experiment, three different times 40, 60 and 80 seconds were used for the tests. The temperature of the test liquid (water) was kept fairly at 25^{o}C. The intensity of the generator was held constant at 100 percent. Immediately after testing, the sample was removed and carefully dried to avoid any mechanical damages using a hand dryer for a period of 5 minutes before placing them in a special holder for further analysis.

(a)

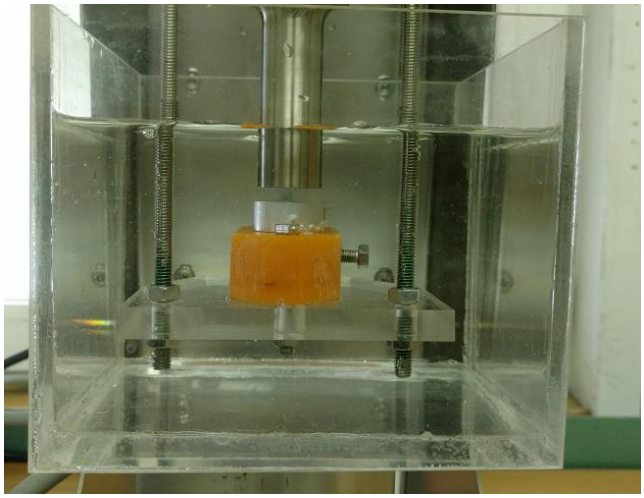

(a)

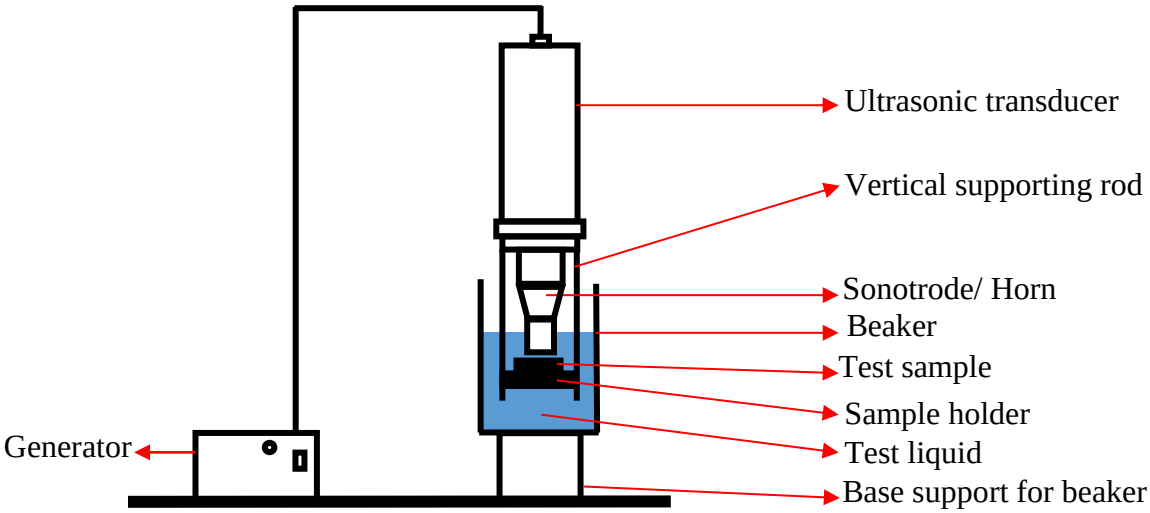

(c)

Figure 16: cavitation apparatus setup, (b) beaker containing sample placed in a holder, (c) schematic description of setup

4.0 Results Evaluation

This chapter describes the various techniques used in the analysis of the pits. The results were obtained using Scanning Electron Microscopy and contact profilometry techniques.

4.1 Results from Scanning Electron Microscope

A brief analysis of SEM micrographs has been done to understand the estimate the number of pits formed as a result of the different exposure times.

4.1.1 Analysis of SEM Micrographs

Micrographs of the samples were obtained from the SEM Zeiss Ultra Plus and different resolutions have been provided for analysis of the pit formation and the extent of damage to the surface of the material. The higher resolutions of the images ensured that the identified pit was visible enough to be analyzed but had a huge drawback because only a few numbers of pits could be observed. In *Figure 18,* the regions marked red could possibly indicate structural defects from manufacturing while the marked regions in white show the deformation of the surface due to pit formation. The distribution of pit diameters varies for all the samples since the pits have different diameters, shapes, and sizes. Some of the pits formed as clusters as the exposure time increased. The loaa od material will likely be more evident as the deformation rate increases with exposure time.

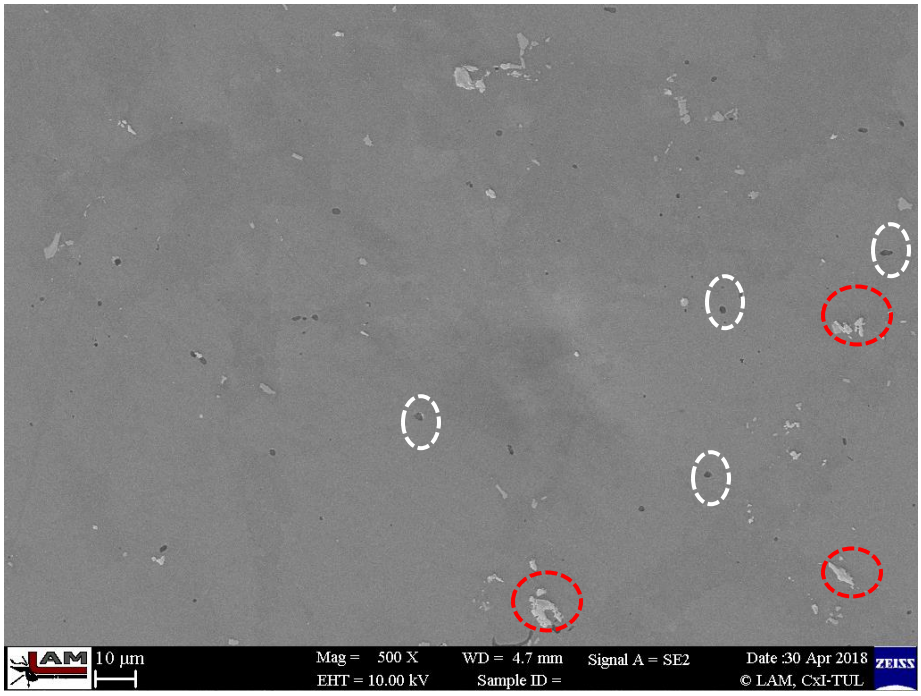

Figure 17: SEM micrograph for the sample after 40 s exposure to cavitation bubbles

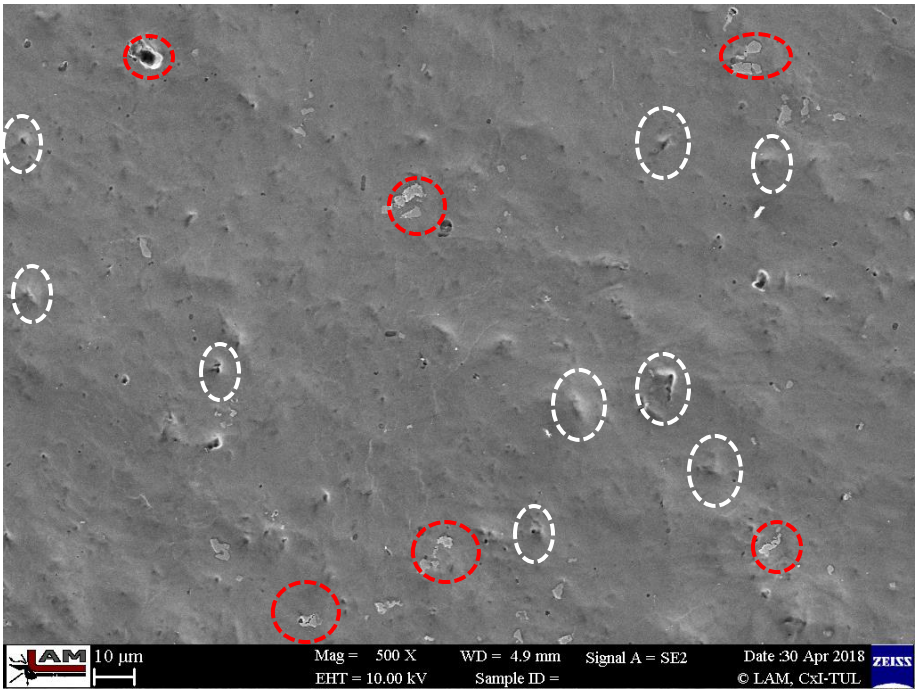

Figure 18: SEM micrograph for the sample after 60 s exposure to cavitation bubbles

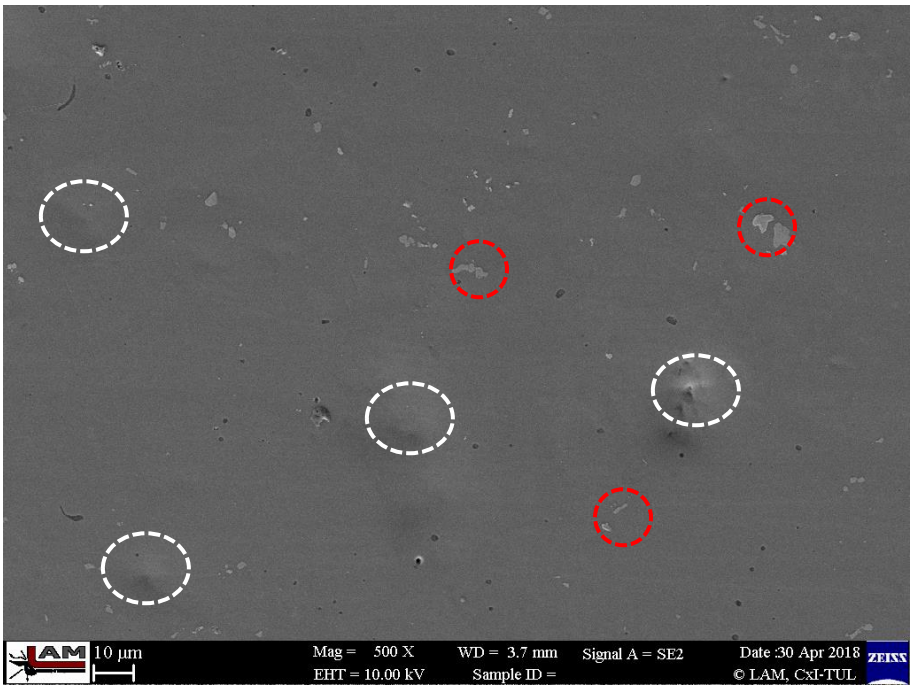

Figure 19: SEM micrograph for the sample after 80 s exposure to cavitation bubbles

4.1.2 Pit Number Estimation on SEM Micrographs

In order to identify the pits with ease, the 500X resolutions of the SEM micrograms were selected. The larger resolution allowed a large number of pits to be observed. Pit diameters and numbers were determined for each sample using the Zeiss 3DSM Metrology software. The surface data was imported into the Mountains Map software and scaled using the original scale on the SEM micrograph as a reference value. The image was then light conditioned before applying a binary segmentation. The segmentation threshold was set to an automatic value selected by the software in order to have the best conditions with lighting. The generated binary image was then morphologically corrected to help identify the pits after and converted to a multicolor image (*Figure 20*b) to allow easy in the identification of the pits. The maximum diameter of each pit was recorded by clicking on the grain. The data was exported and a histogram of the results was plotted. This was repeated for the remaining samples (*Figure 21* and *Figure 22*).

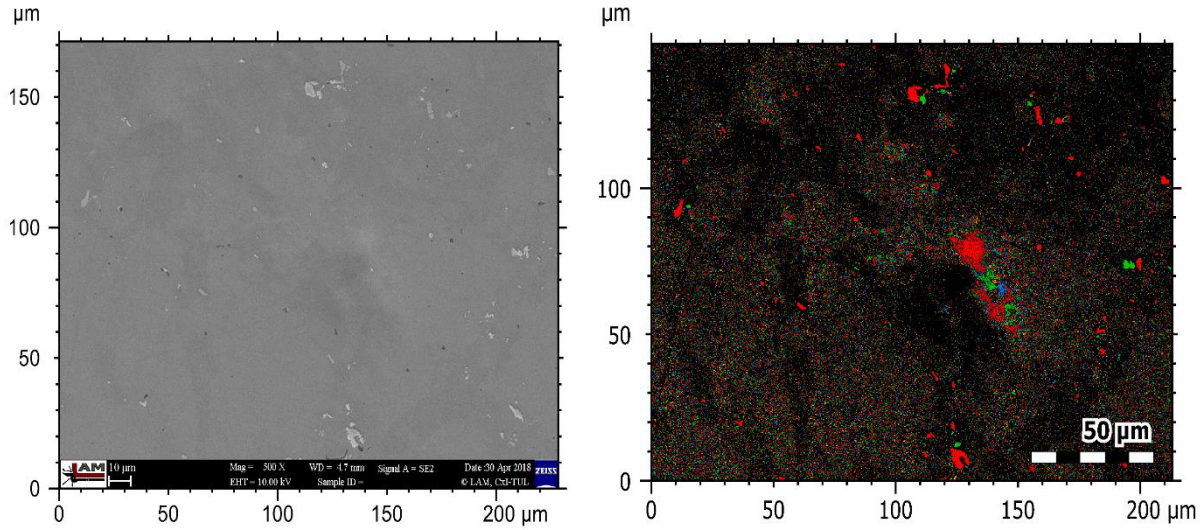

(a) (b)

Figure 20: (a) SEM micrograph of test sample (40 s), (b)Multicolored segmented image (40 s)

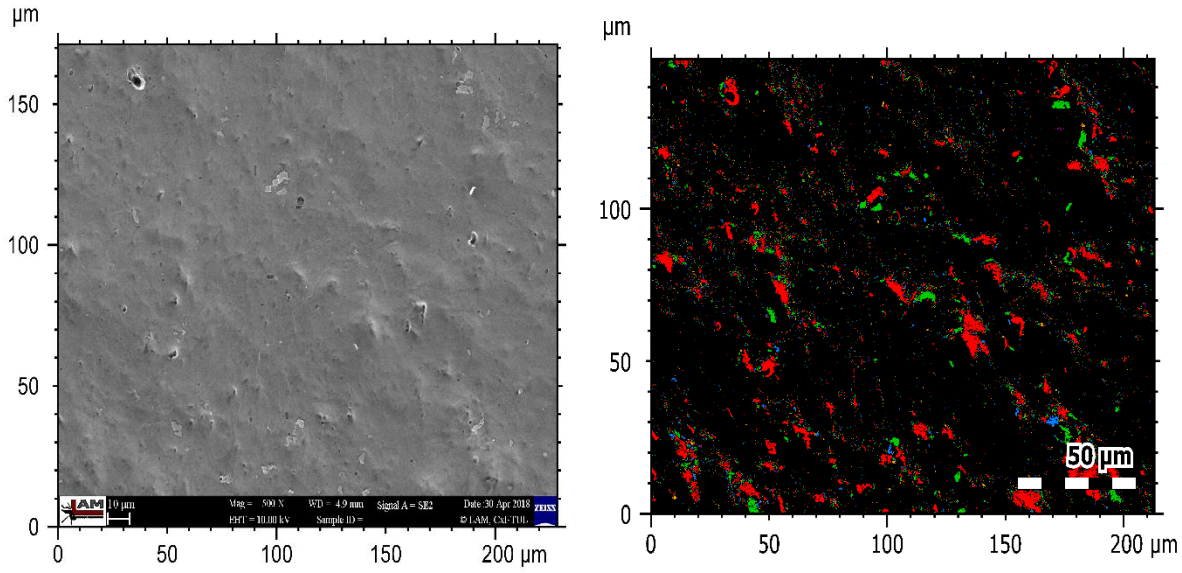

Figure 21: (a) SEM micrograph of test sample (60 s), (b)Multicolored segmented image (60 s)

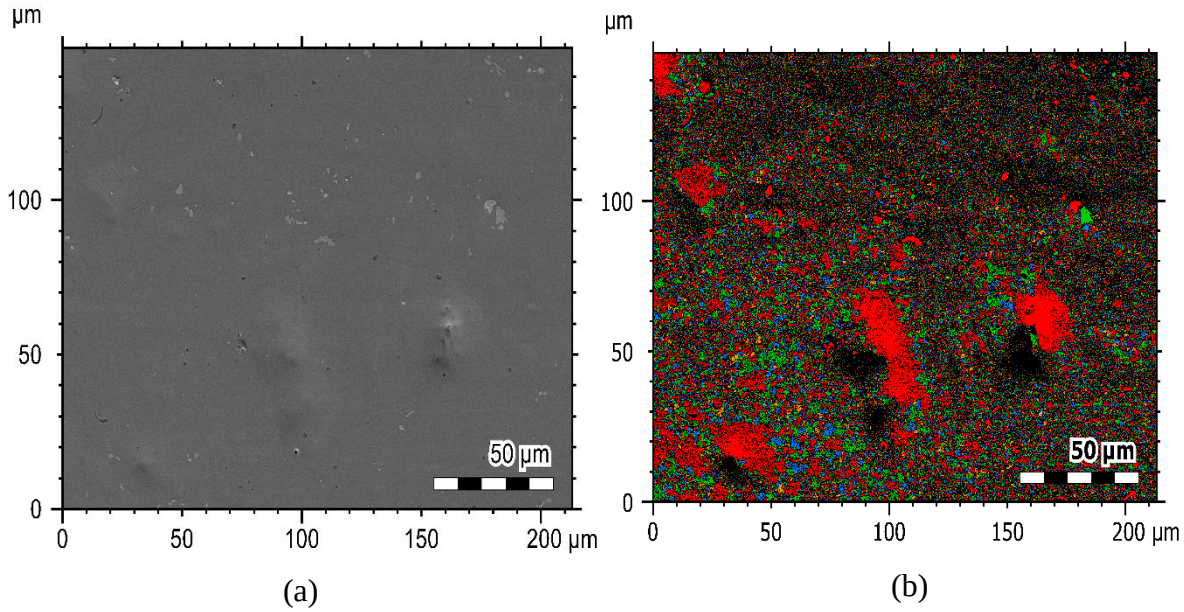

Figure 22: (a) SEM micrograph of test sample (80 s), (b) Multicolored segmented image (80 s)

4.2 Results from Dektak XT Profilometer

In this study, a Dektak XT contact profilometer fitted with a 2 µm stylus was used to assess the topography of the pits. The contact profilometer operated at a speed of 200 µm /s and a stylus force of 5mg. The analyzed surface was approximately 2mm x 2mm. A total of 3001 pts at a resolution of 0.666 um/pts were measured to give a scan length of 2000um. The profile had a map extent of 2000 µm at a resolution of 1um/trace for 2000 traces. The initial 3D surface plot of the topographical data from the profilometer showed the signal to be highly inclined. Signals that have huge tilt angles are difficult to analyze because the reference plane for characterizing the pit geometry will be skewed to one direction. The tilt was corrected by fitting the function with a polynomial function of the ninth (9^{th}) order. This gives residuals without any inclination. The 3D surface plots of the sample before and after preprocessing are shown in (*Figure 23* and *Figure 24*) respectively. The resulting leveled signal helped ensured that a common base plane was used to characterize the pit.

4.2.1 Signal Plane Correction

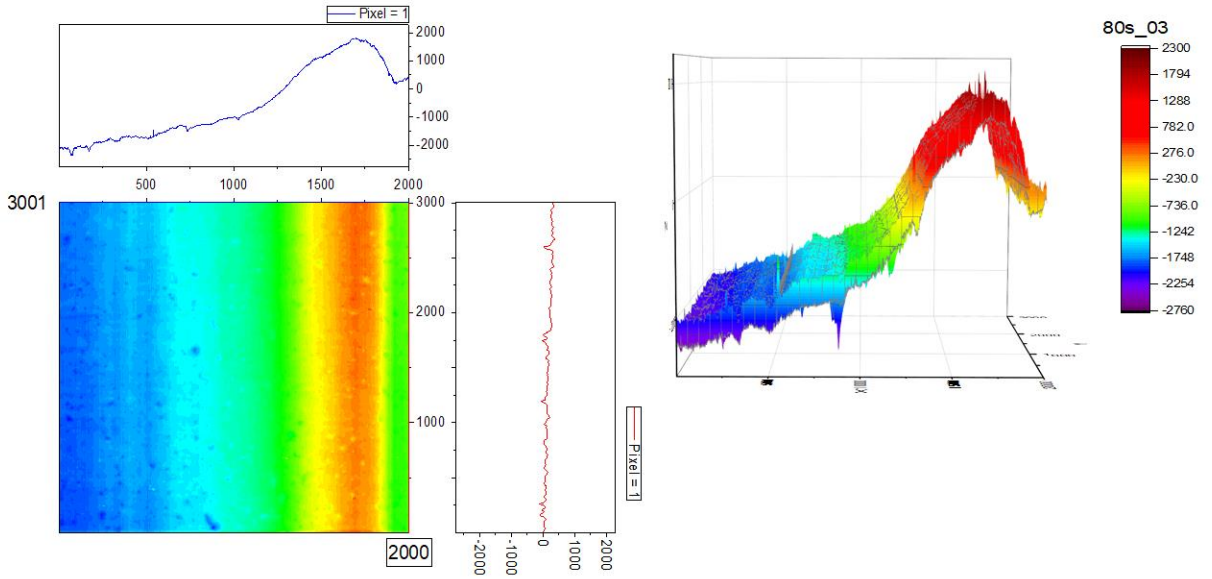

Figure 23: Initial contour profile of sample and 3D colormap surface plot

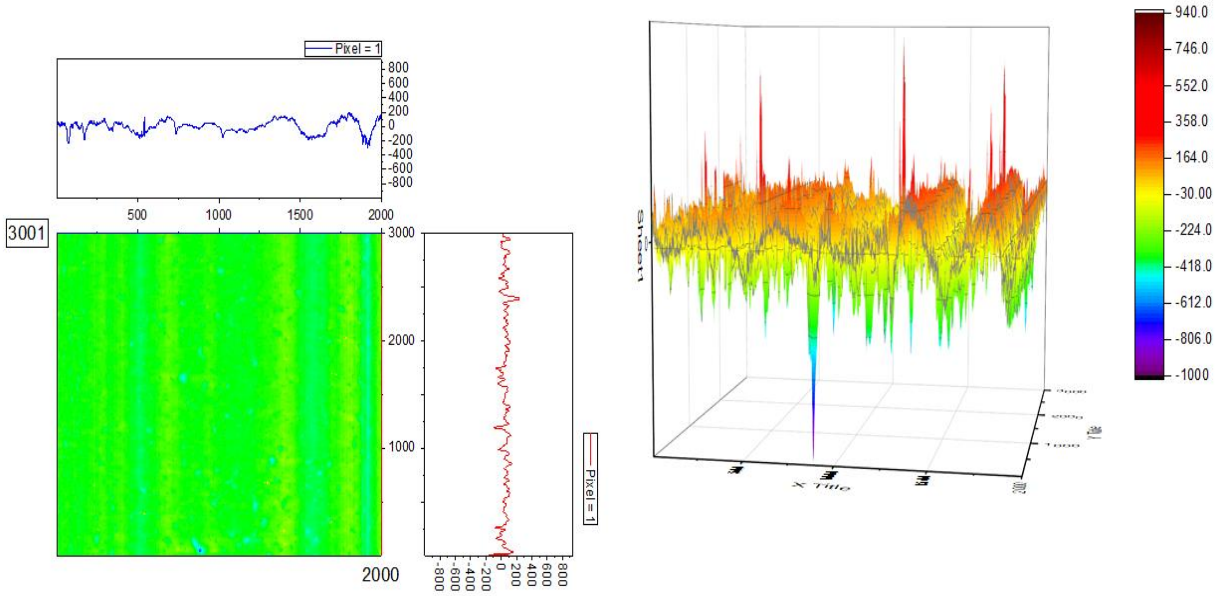

Figure 24: Final contour profile of sample and 3d colormap surface plot

4.2.2 Pit Analysis of Profilometer Data with Matlab

The signals were processed as seen in (Figure 24) and then analyzed using Matlab [63]. The analyzed area of 4 mm^2 was selected to obtain a sufficiently large number of pits for analysis. A cutoff depth was selected to help identify the pits (circled). The value of the cutoff depth is important for the correct estimation of the pit diameter numbers. Erroneously selecting this cutoff value, 0.1 µm, will result in the over-estimation (Figure 25a) of the pit numbers. The cutoff depth value of 0.5 µm resulted in the selection of pits (Figure 25b) that do not merge. Choosing an excessively larger (2µm) cutoff depth eliminated shallow pits as seen in (c). The effects of the cutoff depth on the estimation of the number of impacts against the material is in (Figure 26). It can be seen that choosing a higher cutoff depth value results in less number of pits per the analyzed area. Moreover, as the cutoff depth (0.1 µm) decreases, the pitting rate increases. Therefore 0.5 µm is considered a good choice for the estimation of pit parameters since a sufficiently high number of unmerged pits are selected.

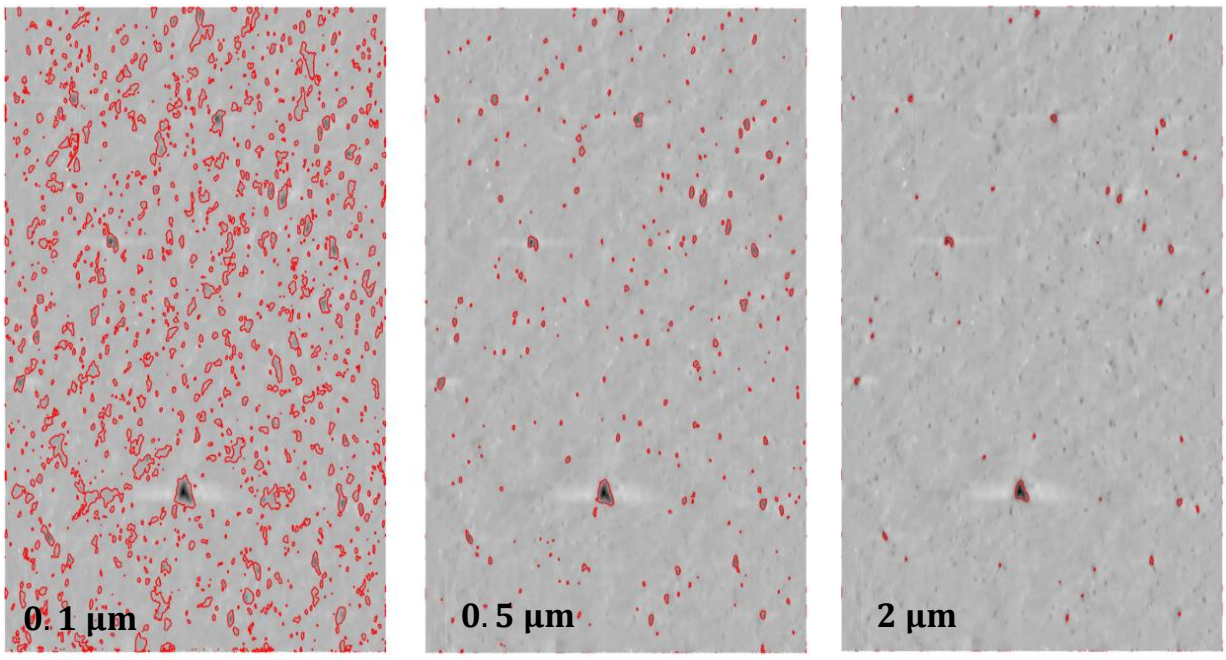

(a) (b) (c)

Figure 25: Influence of cutoff depth on identified pits

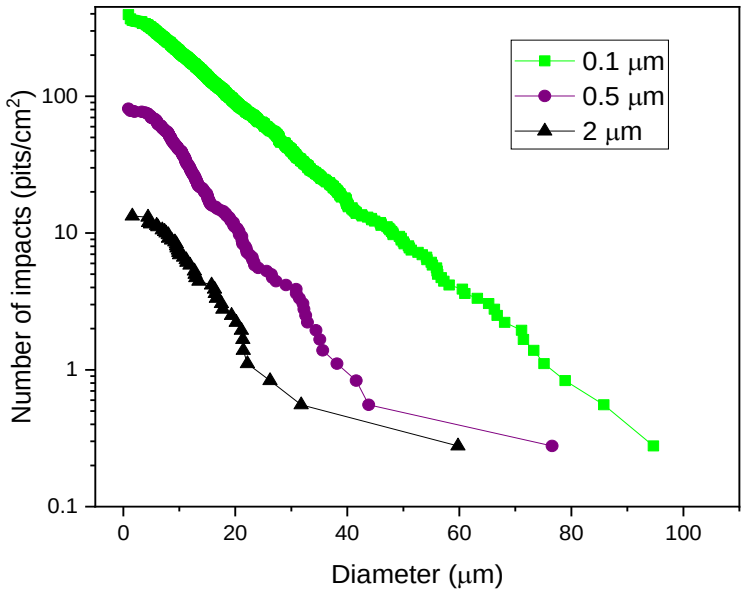

Figure 26: Estimation of the number of impacts for different cutoff depths

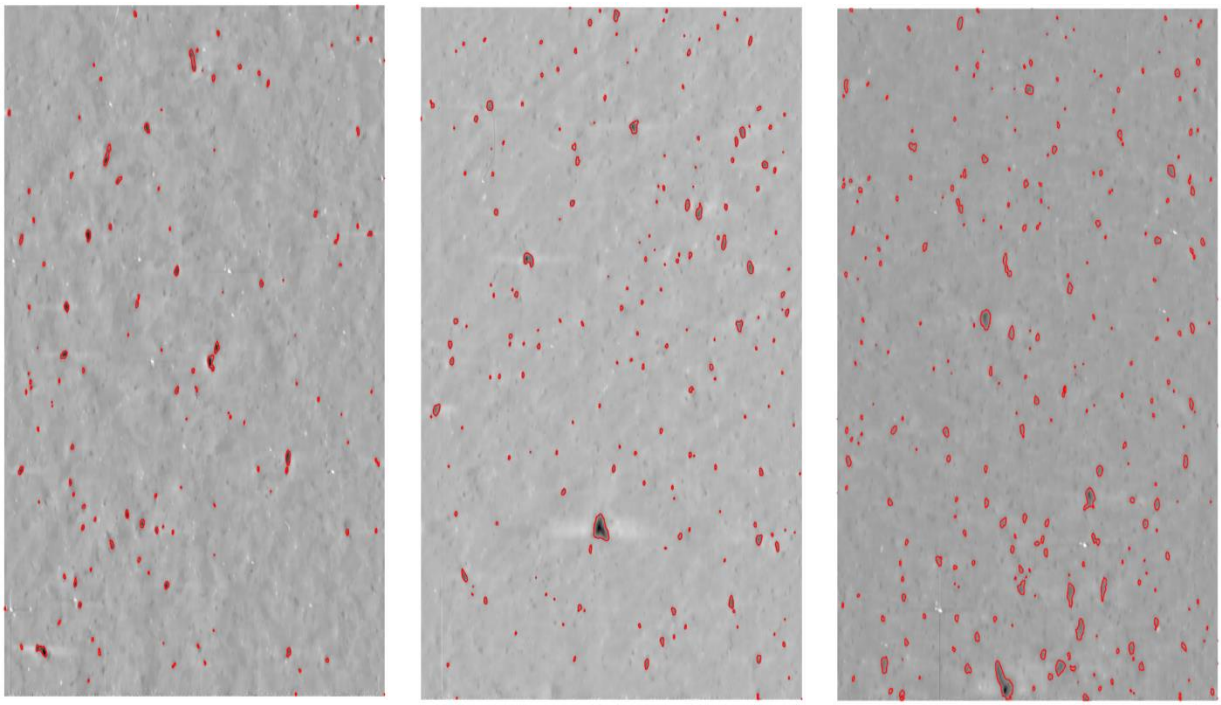

Figure 27: Identification of pits based on exposure times of (a) 40 s, (b)60 s, and (c) 80s

The distribution of the cavitation pits according to its diameter and depth are shown in *Figure 28*, *Figure 29* and *Figure 30*. There is no clear correlation between the pit depth and diameter for each sample because of the random distribution of the two parameters. However, when the three diagrams are compared they showed one unique feature which is a significantly high number of pits occurring at diameters smaller 10 µm after the exposure time of 40s, 20 µm after an exposure of 60s, and finally 30 µm after an exposure time of 80s. The increase in exposure time thus has a linear relation to the numbers of pits created on the surface of the samples. *Figure 30* clearly indicates significant pits with diameters above (60 µm). *Figure 31* shows that a combined distribution of pits depth and diameters from the three samples. It can be seen that larger pit diameters are randomly scattered with varying pit depth. Besides the number of pits created as the exposure time increases, it is difficult to classify the pits diameter according to the depths. This indicates that pits with large diameters do not always correspond to large depths and this conclusion has been shared in other works [63, 65].

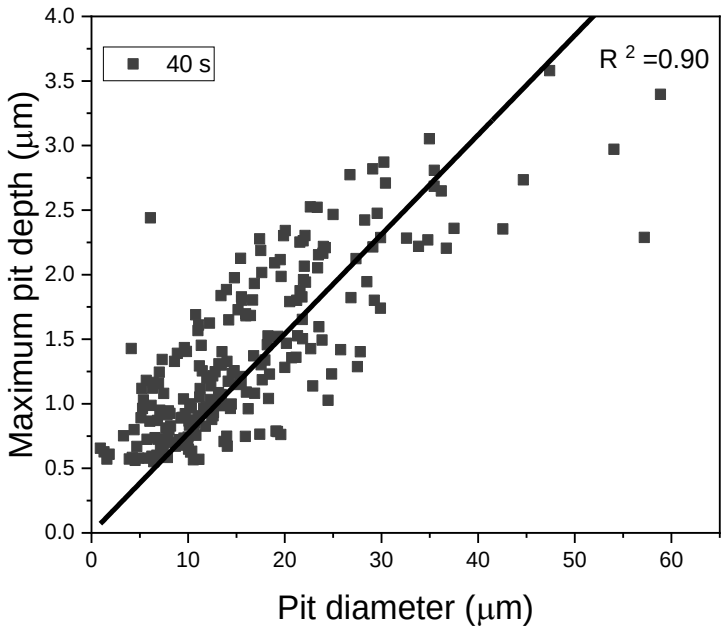

Figure 28: Histogram of pit distribution with pit depth (40 s). (Cutoff depth of 0.5µm)

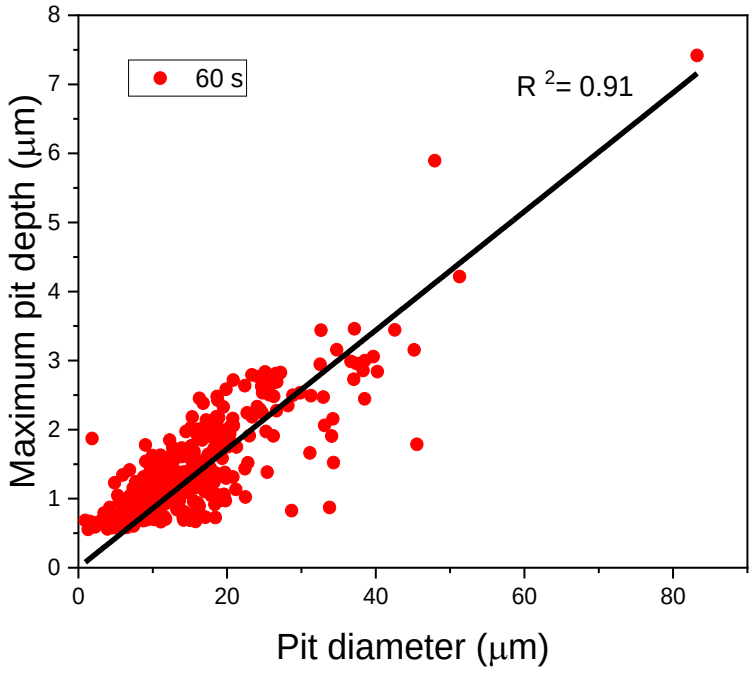

Figure 29 Histogram of pit distribution with pit depth (60 s). (Cutoff depth of 0.5μm)

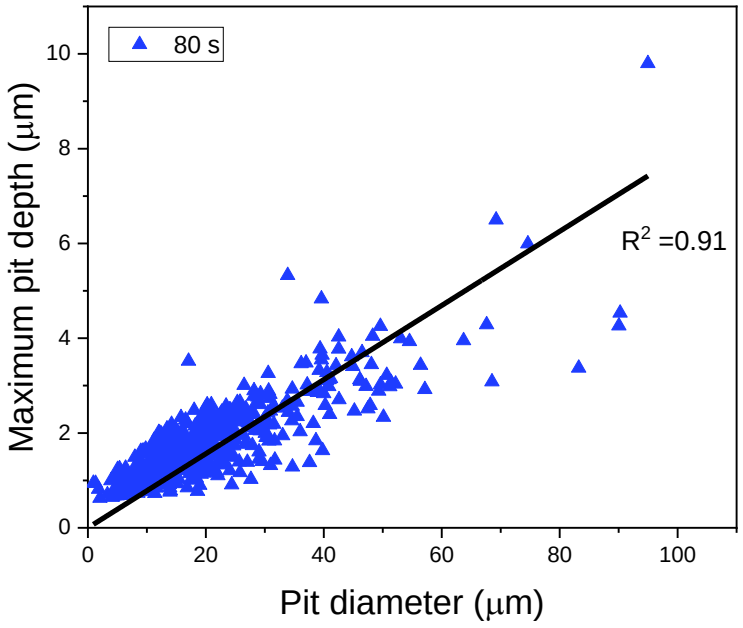

Figure 30 Histogram of pit distribution with pit depth (80 s). (Cutoff depth of 0.5μm)

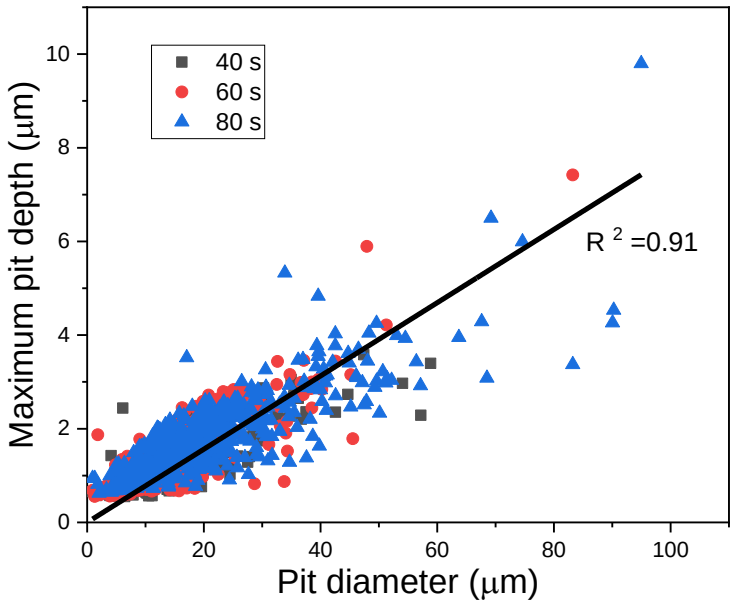

Figure 31: Histogram of pit distribution with pit depth. (Cutoff depth of 0.5μm)

4.2.3 Estimation of Impact Force from Pit Depth and Jet Diameter

From *Table 3*, a simulation was performed in Marc using values from the pit depth and diameter to determine the impact force. It was found that a jet diameter of 10 μm could create a pit depth of approximately 0.95 μm with an impact force of 0.63 N and a corresponding pressure of 7.99 GPa. The same jet diameter (10 μm) could also generate a much bigger depth of around 2 μm but this will require a significantly high impact force of nearly 1.14 N. The force required to create any pit depth can be computed. For example, a pit depth of 0.93 um can also be generated by a 30 μm jet diameter using an estimated impact force of 6.09 N. This indicates that the depth or deformation created on the material surface does not have a high correlation with jet diameter. however, the force exerted on the material as well as the material properties at that particular point on impact determines the depths created.

Table 3: Simulation to determine impact force for a given pit depth

Jet Diameter	Pit Depth (Resulting deformation)	Maximum Force	Maximum Pressure
μm	μm	N	GPa
10	0.95	0.63	7.99
10	1.97	1.14	14.51
30	0.93	6.09	8.61
30	1.96	10.82	15.31

4.2.4 Number of Pit Diameters

In *Figure 32*, the probability of generating pits with a diameter above 40 µm are less. As the exposure time increases to 60 s, the number of pits increase but diameters above 60 µm have low probabilities of occurrence. *Figure 33* has a higher probability of generating pits with diameters less than 45 µm but showed no pits between the diameters of 60 and 80. *Figure 34* shows pits generated after 80 s and has a significantly higher number of pits below 70 µm but pits with diameters above 70 µm have a low probability of occurrence.

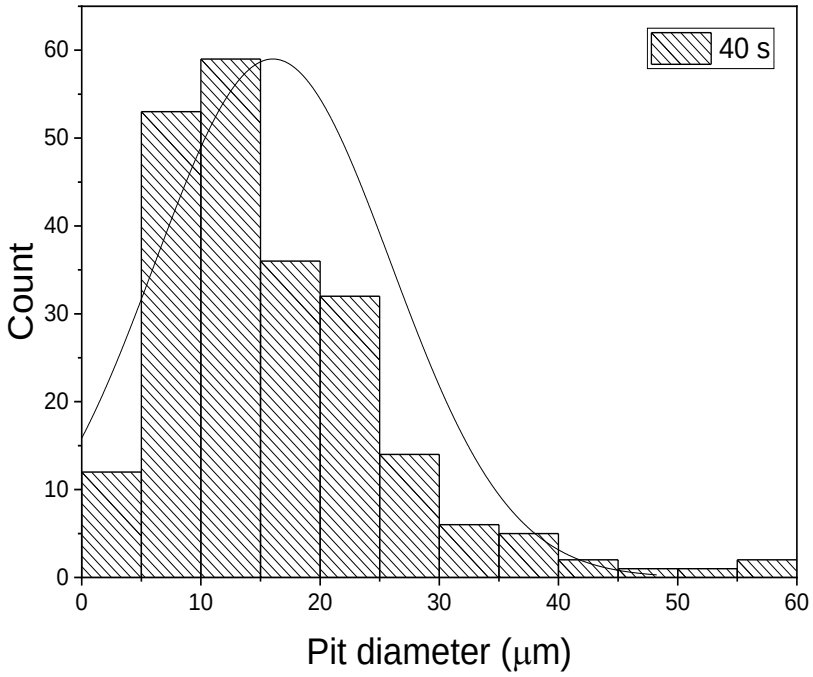

Figure 32: Histogram of the pit diameter distribution (40 s). (cutoff depth of 0.5μm)

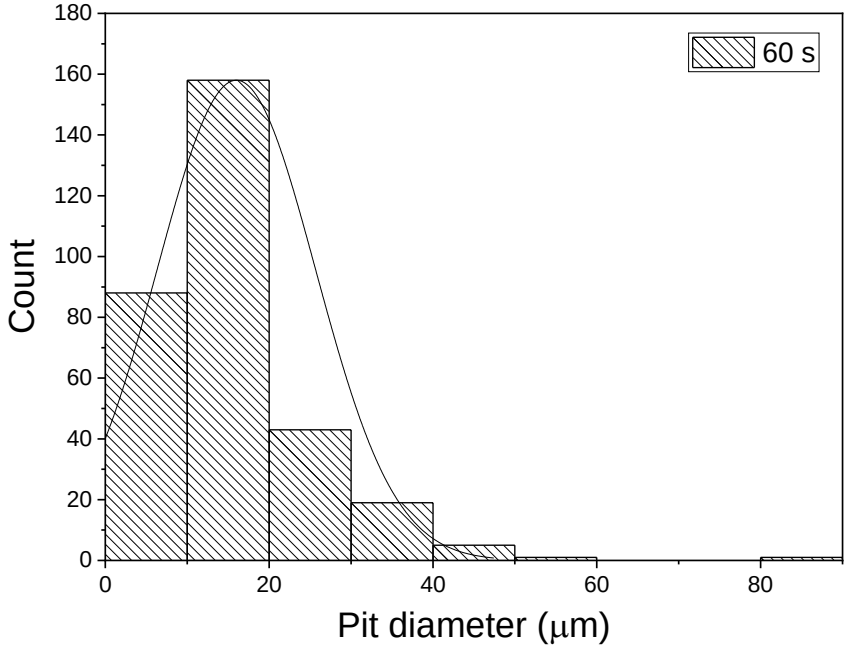

Figure 33: Histogram of the pit diameter distribution (60 s). (cutoff depth of 0.5μm)

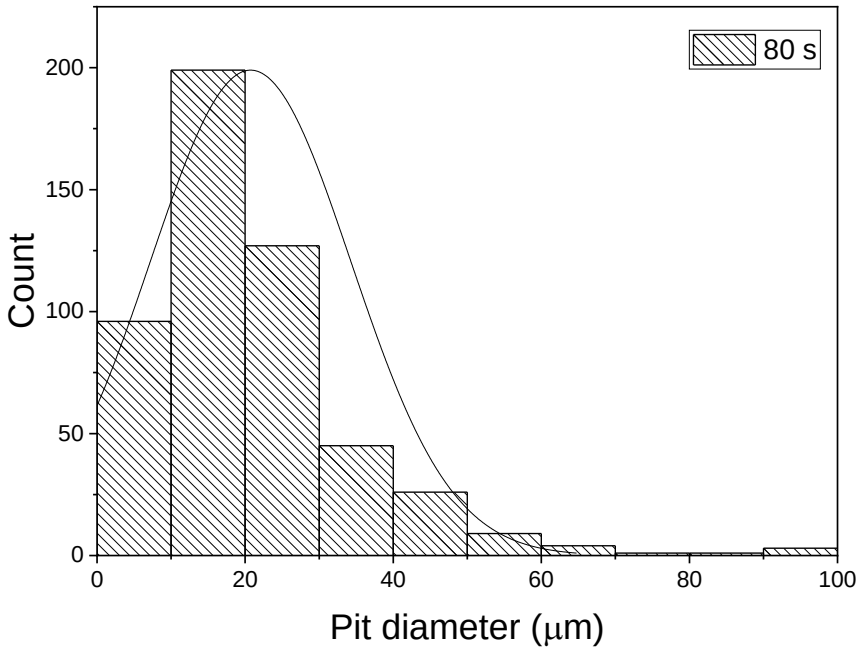

Figure 34: Histogram of the pit diameter distribution (80 s). (cutoff depth of 0.5μm)

4.2.5 Dependence of Cumulative Number of Impacts and Pit Volume on Pit Diameter

In *Figure 35*, the cumulative number of impacts is highest for pits with the smaller diameter and reduces as the diameter increases. This relation indicates an inverse proportionality between the number of impacts and pit diameter in a single time exposure. As the exposure time increases, the number of impacts also significantly increases when two different exposure times are compared. The sample exposed to 40 s of cavitation produced the least number of pits recorded by the profilometer. The gradual increase of exposure time to 60 s shows the significantly higher number of impacts as well as pits with much bigger diameters. After 80 s, the number of pits is seen to be at its highest and again produces pits with much bigger diameters as compared to pits with 60 exposure times.

In *Figure 36*, a higher pitting rate is observed in the sample with the highest exposure time. The number of diameters with bigger diameters are seen to increase with an increase in exposure time. Within the same exposure time, the number of impacts decreases with increasing diameter. This

means that the number of pits with bigger diameters will be less as compared to smaller sized diameters. The pattern overserved agrees with to the results in *Figure 35*. Both Sem and profilometry techniques can be used to quantify the pits numbers and diameters since the results of each method are in agreement. Fewer pits were recorded from the SEM micrographs because of the higher resolution used which analyzed a very small area approximately 0.03 mm^2. The small area showed that each micrograph only showed fewer number of pits per analyzed area.

In *Figure 37*, a good correlation exists between the pit volume and diameter with an R^2 value of 0.96. This relation is not totally dependent on the exposure time but may depend instead on the material property. From the diagram, we can relate the pit volume as a power law to the pit diameter by $v \propto D^{2.2}$. This is only valid as an average approximation of the equivalent diameter because significant deviations can occur. The relation was modelled using the allometric power law.

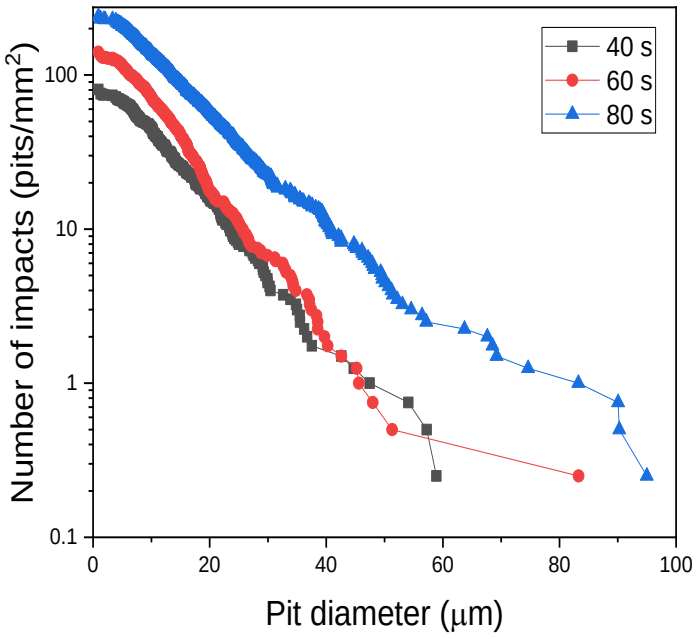

Figure 35: Cumulative number of pits per diameter obtained from surface profilometry (cutoff depth: 0.5)

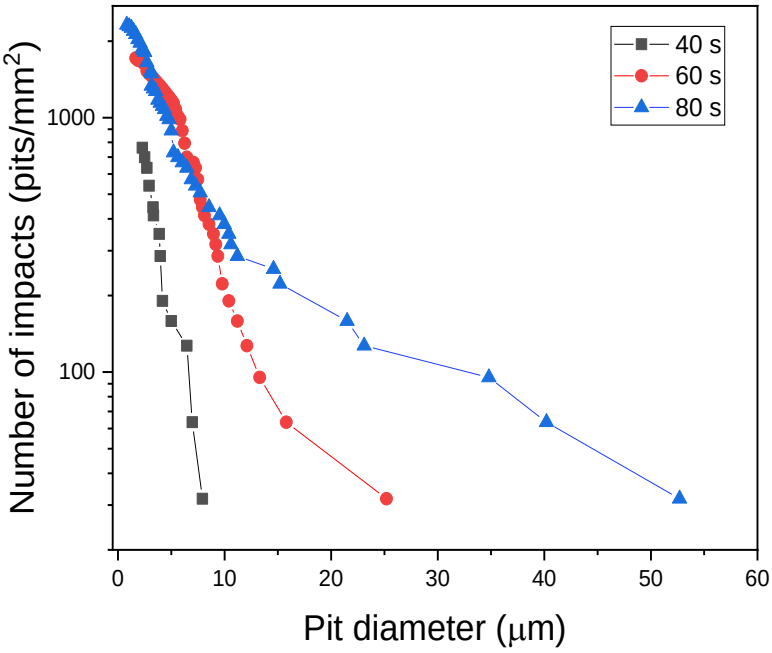

Figure 36: Cumulative number of pits per diameter obtained from SEM (cutoff depth: 0.5)

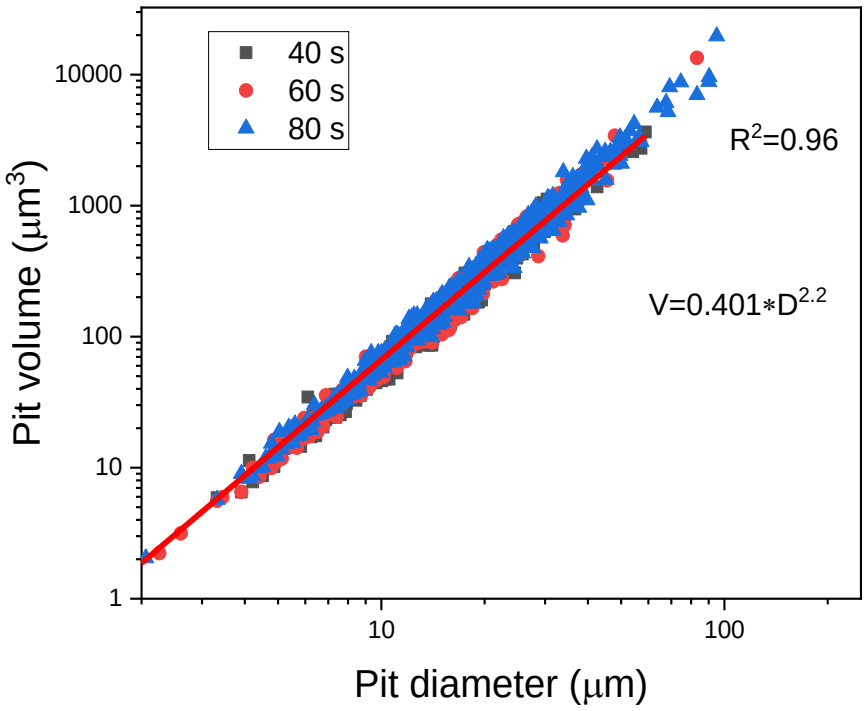

Figure 37: Pit volume as a function of different exposure times obtained from surface profilometry

In *Figure 38*, the formation of pits with bigger volumes decrease within the same exposure time. It can be seen that the exposure time is a function of the pits numbers formed. The volumes of pits formed at much higher exposure time are seen to be more than the shorter times however the distribution of volumes with much bigger volumes are seen to have a very small pitting rate.

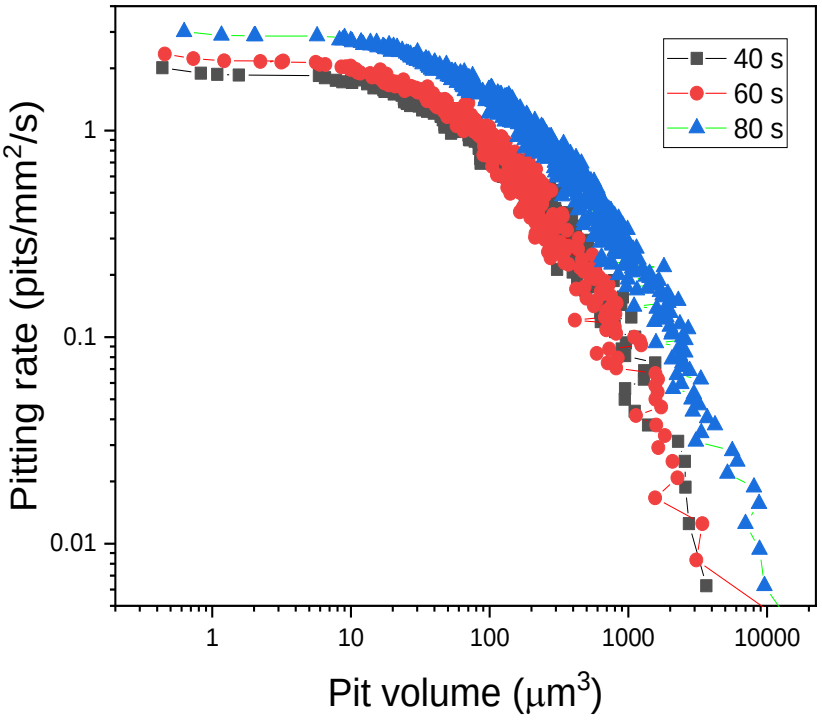

Figure 38: Pitting rate as a function of Pit volume obtained from surface profilometry (Cutoff depth: 0.5 um)

5.0 Results Discussion

The discussion of the results will be based on the two different techniques used in the analysis of the pits. The SEM technique revealed an increase in pit numbers as the exposure time increased. The longest exposure time revealed much bigger diameters than the samples which were exposed to the pitting test at shorter durations. The advantage of this technique allowed us to visualize the shapes of the pits and the ability to characterize each pit for the measurements of diameter and area.

The data from the profilometer was used to estimate the number of pits and to characterize the distribution of pit diameter, depth and volume using a suitably determined cutoff depth. If pits clusters can be avoided, then the pitting rate should be expected to be proportional to the exposure time. This is only true if material properties of the sample remain fairly constant within the exposure time and cavitation bubbles are generated in a stable fluid flow. The region around a pit is larger than the pit and considered to be plastically deformed. The avoidance of pit clusters prevents the hardening of the material by the impacting pressure wave. Additionally, if new pits form in newer regions it ensures that similar impacts result in similar deformation helping avoid aging effects. In this way, a small area can be analyzed and used to estimate the deformation rate for the entire surface.

While pit formation depends mostly on the intensity of the cavitation pressure wave, the properties of the material can be considered to play a significant role in the pit formation. If the material is strong enough to withstand the stresses from the repeated loading, then the material may recover from the elastic deformations. Within a plastic region, high stresses impacted on the material will cause significant damages which is irreversible. The influence of the exposure time on the number of pits as established presents a way to predict the extent of damage to the material. The initial onset of cavitation known as the incubation phase does not involve any material loss. The distribution of pit diameter is seen to increase in number as the exposure time increases. The initial phase of pitting usually starts with the formation of a large number of small-sized pits on the surface of the material. Pitting rate is seen to increase with high exposure time but the formation of larger volumes reduces as the pitting rate increases. The reason could be due to the work hardening of the material by the impacting pressure waves. This could significantly increase the strength of the material to withstand further losses. As the exposure time increases, the chance of

forming much larger deformations in the same area will likely lead to the formation of pits with much bigger volumes. Since the volume is directly proportional to the diameter, we expect much bigger diameters in an extended exposure time as compared to much shorter times when a surface is exposed to cavitation pressure pulses. Pits may merge around their ends to form much bigger pits. Plastic deformation around these large pits results in much larger deformation of the material as a whole. The longer the material operates in conditions which expose the surface to the effects of bubble impacts, the faster its surfaces erode. It is expected that the exposure time can be linked directly to significant mass loss from the material. Additionally, the distribution of pit diameter and pit depth showed that larger diameters do not always correspond to bigger pits. The reason may be that pits with different shapes form making it difficult to estimate the depths of each pit by its diameter. This is however independent of the operating conditions.

The simulation carried out in Marc in order to determine the magnitude of the impact force presents a model to understand the relationship between pit depth, jet diameter and impact force. It has been determined that the depth or deformation of the material surface is significantly affected by the magnitude of the impact force. Bigger pit depths require a higher impact force. Different jet diameters will require different impact force to create an extensive deformation in the material.

The SEM technique is a powerful visualization technique but requires an expert to analyze the data. At lower resolutions, it is, however, unable to capture the extent of the damage on the surface of the material. Repeated measurement along the entire surface may be required to be done to prove that the damage is uniform. The contact profilometer, however, can scan a considerably large enough area for comprehensive analyze. The data from the surface profile can be processed to estimate pit number, diameter, volume and depth of deformation. The information can then be used to characterize the pits.

6.0 Conclusion

The current study researched on the cavitation bubble interaction and highlighted the effects of the impact of cavitation pressure waves on material properties. The experiment was carried out using the vibratory cavitation device to perform pitting test during incubation period. Three different exposure times were selected to study the intensity of cavitation bubble-wall interaction. The results were evaluated using two separate techniques to show the influence of exposure time on the number of pits as well as the distribution of diameter and volume. The influence of the pitting rate and the number of impacts have on pit diameter have been compared using the two different techniques. The number of pits has been compared for different exposure times. It has been found that the power law gives a good approximation of the dependency of pit volumes on diameter. Pitting tests provide a fast approach to characterize pit formation according to depth, volume, diameter and number. The Scanning Electron Microscope offered a highly magnified image characterize the pit shape and size. However, because of the small area analyzed it is not recommended for proper statistical evaluation of the pits. The profilometry techniques is also a useful technique to study the relationship between the above-mentioned parameters because a large area can be analyzed. Further understanding of material properties and testing conditions such as properties of the test liquid and its temperature should be considered to accurately predict material damage as a result of cavitation.

References

[1] PALAKODATY, Srinivas a Peter YORK. Phase Behavioral Effects on Particle Formation Processes Using Supercritical Fluids. *Pharmaceutical Research* [online]. 1999, **16**(7), 976–985. ISSN 1573-904X. Dostupné z: doi:10.1023/A:1011957512347

[2] REBOUD, Jean-Luc, Benoit STUTZ a Olivier COUTIER. Two phase flow structure of cavitation: experiment and modeling of unsteady effects. In: *3rd International Symposium on Cavitation CAV1998, Grenoble, France*. 1998.

[3] KUNZ, Robert F, David A BOGER, Thomas S CHYCZEWSKI, D STINEBRING, H GIBELING a T R GOVINDAN. Multi-phase CFD analysis of natural and ventilated cavitation about submerged bodies. In: *Proceedings of FEDSM*. 1999.

[4] PLESSET, Milton S. The dynamics of cavitation bubbles. *Journal of applied mechanics*. 1949, **16**, 277–282. ISSN 0021-8936.

[5] WAN, Mingxi, Yi FENG a Gail TER HAAR. *Cavitation in Biomedicine*. B.m.: Springer, 2015. ISBN 940177255X.

[6] CHOI, Min Joo, Gwansuk KANG a Jung Sik HUH. Geometrical characterization of the cavitation bubble clouds produced by a clinical shock wave device. *Biomedical Engineering Letters*. 2017, 1–9. ISSN 2093-9868.

[7] ASIF, Saira, Lai Fatt CHUAH, Jiří Jaromír KLEMEŠ, Mushtaq AHMAD, Majid Majeed AKBAR, Keat Teong LEE a Anmol FATIMA. Cleaner production of methyl ester from non-edible feedstock by ultrasonic-assisted cavitation system. *Journal of Cleaner Production*. 2017. ISSN 0959-6526.

[8] AZAR, Lawrence. Cavitation in ultrasonic cleaning and cell disruption. *Controlled Environments February*. 2009, 14–17.

[9] MAISONHAUTE, Emmanuel, Cesar PRADO, Paul C WHITE a Richard G COMPTON. Surface acoustic cavitation understood via nanosecond electrochemistry. Part III: Shear stress in ultrasonic cleaning. *Ultrasonics sonochemistry*. 2002, **9**(6), 297–303. ISSN 1350-4177.

[10] METTIN, R, I AKHATOV, U PARLITZ, C D OHL a W LAUTERBORN. Bjerknes forces between small cavitation bubbles in a strong acoustic field. *Physical Review E* [online]. 1997, **56**(3), 2924–2931. Dostupné z: https://link.aps.org/doi/10.1103/PhysRevE.56.2924

[11] MISHRA, Chandan a Yoav PELES. Cavitation in flow through a micro-orifice inside a silicon microchannel. *Physics of fluids*. 2005, **17**(1), 13601. ISSN 1070-6631.

[12] BLAKE, John R a D C GIBSON. Cavitation bubbles near boundaries. *Annual review of fluid mechanics*. 1987, **19**(1), 99–123. ISSN 0066-4189.

[13] SHAH, Yatish T, A B PANDIT a V S MOHOLKAR. *Cavitation reaction engineering*. B.m.: Springer Science & Business Media, 2012. ISBN 1461547873.

[14] PLESSET, Milton S. Cavitating flows. 1969.

[15] CHUDINA, M. Noise as an indicator of cavitation in a centrifugal pump. *Acoustical Physics* [online]. 2003, **49**(4), 463–474. ISSN 1562-6865. Dostupné z: doi:10.1134/1.1591303

[16] MILLER, Douglas L, Sorin V PISLARU a James F GREENLEAF. Sonoporation: Mechanical DNA Delivery by Ultrasonic Cavitation. *Somatic Cell and Molecular Genetics* [online]. 2002, **27**(1), 115–134. ISSN 1572-9931. Dostupné z: doi:10.1023/A:1022983907223

[17] WALKER, R. Ultrasound improves electrolytic recovery of metals. *Ultrasonics Sonochemistry* [online]. 1997, **4**(1), 39–43. ISSN 1350-4177. Dostupné z: doi:https://doi.org/10.1016/S1350-4177(96)00035-1

[18] TROCK, Bernard. *A Study of Cavitation Erosion*. B.m.: SAE Technical Paper. 1956.

[19] STEPANOFF, A J. Cavitation in Centrifugal Pumps. *TRANS. ASME*. 1945, **67**, 539–552.

[20] KNAPP, Robert T. Cavitation mechanics and its relation to the design of hydraulic equipment. *Proceedings of the Institution of Mechanical Engineers*. 1952, **166**(1), 150–163. ISSN 0020-3483.

[21] PIELEMEIER, W H. Some Effects of Cavitation near 30 cps. *The Journal of the*

Acoustical Society of America. 1951, **23**(2), 224–228. ISSN 0001-4966.

[22] DEAN, Robert B. The formation of bubbles. *Journal of Applied Physics*. 1944, **15**(5), 446–451. ISSN 0021-8979.

[23] PLESSET, M S a A T ELLIS. On the mechanism of cavitation damage. *Transactions of the ASME*. 1955, **77**, 1055–1064.

[24] KORNFELD, M a L SUVOROV. On the destructive action of cavitation. *Journal of Applied Physics*. 1944, **15**(6), 495–506. ISSN 0021-8979.

[25] RAYLEIGH, Lord. VIII. On the pressure developed in a liquid during the collapse of a spherical cavity. *The London, Edinburgh, and Dublin Philosophical Magazine and Journal of Science*. 1917, **34**(200), 94–98. ISSN 1941-5982.

[26] KNAPP, Robert T. Recent investigations of the mechanics of cavitation and cavitation damage. *Transactions of the ASME*. 1955, **77**, 1045–1054.

[27] LAUTERBORN, W a H BOLLE. Experimental investigations of cavitation-bubble collapse in the neighbourhood of a solid boundary. *Journal of Fluid Mechanics* [online]. 2006/03/01 vyd. 1975, **72**(2), 391–399. ISSN 0022-1120. Dostupné z: doi:DOI: 10.1017/S0022112075003448

[28] PLESSET, Milton S a Richard B CHAPMAN. Collapse of an initially spherical vapour cavity in the neighbourhood of a solid boundary. *Journal of Fluid Mechanics*. 1971, **47**(2), 283–290. ISSN 1469-7645.

[29] PLESSET, Milton S a Andrea PROSPERETTI. Bubble dynamics and cavitation. *Annual review of fluid mechanics*. 1977, **9**(1), 145–185. ISSN 0066-4189.

[30] KIM, Ki-Han, Georges CHAHINE, Jean-Pierre FRANC a Ayat KARIMI. *Advanced experimental and numerical techniques for cavitation erosion prediction*. B.m.: Springer, 2014. ISBN 9401785392.

[31] SUPPONEN, Outi, Danail OBRESCHKOW, Philippe KOBEL a Mohamed FARHAT. Detailed jet dynamics in a collapsing bubble. In: *Journal of Physics: Conference Series*. B.m.: IOP Publishing, 2015, s. 12038. ISBN 1742-6596.

[32] MOMMA, T a A LICHTAROWICZ. A study of pressures and erosion produced by collapsing cavitation. *Wear*. 1995, **186**, 425–436. ISSN 0043-1648.

[33] VOGEL, Alfred, S BUSCH a U PARLITZ. Shock wave emission and cavitation bubble generation by picosecond and nanosecond optical breakdown in water. *The Journal of the Acoustical Society of America*. 1996, **100**(1), 148–165. ISSN 0001-4966.

[34] MÜLLER, M, J HUJER, M KOTEK a P ZIMA. Identification of collapse patterns of cavitation bubbles close to a solid wall. In: *EPJ Web of Conferences*. B.m.: EDP Sciences, 2013, s. 1120. ISBN 2100-014X.

[35] PHILIPP, A a W LAUTERBORN. Cavitation erosion by single laser-produced bubbles. *Journal of Fluid Mechanics*. 1998, **361**, 75–116. ISSN 1469-7645.

[36] TONG, R P, W P SCHIFFERS, S J SHAW, J R BLAKE a D C EMMONY. The role of 'splashing'in the collapse of a laser-generated cavity near a rigid boundary. *Journal of Fluid Mechanics*. 1999, **380**, 339–361. ISSN 1469-7645.

[37] SHIMA, A, K TAKAYAMA, Y TOMITA a N MIURA. An experimental study on effects of a solid wall on the motion of bubbles and shock waves in bubble collapse. *Acta Acustica united with Acustica*. 1981, **48**(5), 293–301. ISSN 1610-1928.

[38] ZONG, Yujin, Shanshan XU, Tom MATULA a Mingxi WAN. Cavitation-Enhanced Mechanical Effects and Applications. In: *Cavitation in Biomedicine*. B.m.: Springer, 2015, s. 207–263.

[39] KARIMI, A, M MAAMOURI a J L MARTIN. Cavitation-erosion-induced microstructures in copper single crystals. *Materials Science and Engineering: A*. 1989, **113**, 287–296. ISSN 0921-5093.

[40] GAO, X.-L., X N JING a G SUBHASH. Two new expanding cavity models for indentation deformations of elastic strain-hardening materials. *International Journal of Solids and Structures* [online]. 2006, **43**(7), 2193–2208. ISSN 0020-7683. Dostupné z: doi:https://doi.org/10.1016/j.ijsolstr.2005.03.062

[41] POLA, Annalisa, Lorenzo MONTESANO, Marialaura TOCCI a Giovina Marina LA VECCHIA. Influence of Ultrasound Treatment on Cavitation Erosion Resistance of AlSi7

Alloy. *Materials*. 2017, **10**(3), 256.

[42] DEVI, Prabhavathi, L A BETHALA, Katkam N GANGADHAR, Potharaju S SAI PRASAD, Bulusu JAGANNADH a Rachapudi B N PRASAD. A Glycerol-based Carbon Catalyst for the Preparation of Biodiesel. *ChemSusChem*. 2009, **2**(7), 617–620. ISSN 1864-564X.

[43] JAYAPRAKASH, Arvind, Jin-Keun CHOI, Georges L CHAHINE, Farrel MARTIN, Martin DONNELLY, Jean-Pierre FRANC a Ayat KARIMI. Scaling study of cavitation pitting from cavitating jets and ultrasonic horns. *Wear*. 2012, **296**(1-2), 619–629. ISSN 0043-1648.

[44] SUN, Z, X Q KANG a X H WANG. Experimental system of cavitation erosion with water-jet. *Materials & design*. 2005, **26**(1), 59–63. ISSN 0261-3069.

[45] SOYAMA, Hitoshi. Effect of nozzle geometry on a standard cavitation erosion test using a cavitating jet. *Wear*. 2013, **297**(1-2), 895–902. ISSN 0043-1648.

[46] SOYAMA, H, J D PARK a M SAKA. Use of cavitating jet for introducing compressive residual stress. *Journal of manufacturing science and engineering*. 2000, **122**(1), 83–89. ISSN 1087-1357.

[47] ABOUEL-KASEM, A, B SALEH, K M EMARA a S M AHMED. Characterization of Cavitation Eroded Surfaces at Different Temperatures Using Wavelet Method. *Journal of Tribology*. 2017, **139**(3), 32301. ISSN 0742-4787.

[48] TZANAKIS, I, Leandro BOLZONI, D G ESKIN a M HADFIELD. Evaluation of Cavitation Erosion Behavior of Commercial Steel Grades Used in the Design of Fluid Machinery. *Metallurgical and Materials Transactions A*. 2017, **48**(5), 2193–2206. ISSN 1073-5623.

[49] SREEDHAR, B K, S K ALBERT a A B PANDIT. Cavitation damage: Theory and measurements–A review. *Wear*. 2017, **372**, 177–196. ISSN 0043-1648.

[50] FUTAKAWA, M, H KOGAWA, R HINO, H DATE a H TAKEISHI. Erosion damage on solid boundaries in contact with liquid metals by impulsive pressure injection. *International Journal of Impact Engineering*. 2003, **28**(2), 123–135. ISSN 0734-743X.

[51] SHCHUKIN, Dmitry G, Ekaterina SKORB, Valentina BELOVA a Helmuth MÖHWALD. Ultrasonic cavitation at solid surfaces. *Advanced Materials*. 2011, **23**(17), 1922–1934. ISSN 1521-4095.

[52] SOYAMA, Hitoshi a Masatoshi FUTAKAWA. Estimation of incubation time of cavitation erosion for various cavitating conditions. *Tribology letters*. 2004, **17**(1), 27–30. ISSN 1023-8883.

[53] WANG, Yi-Chun, Ching-Hung HUANG, Yung-Chun LEE a Ho-Hsun TSAI. Development of a PVDF sensor array for measurement of the impulsive pressure generated by cavitation bubble collapse. *Experiments in fluids*. 2006, **41**(3), 365–373. ISSN 0723-4864.

[54] VOGEL, A a W LAUTERBORN. Acoustic transient generation by laser-produced cavitation bubbles near solid boundaries. *The Journal of the Acoustical Society of America*. 1988, **84**(2), 719–731. ISSN 0001-4966.

[55] SOYAMA, Hitoshi, Yuichi SEKINE a Kenichi SAITO. Evaluation of the enhanced cavitation impact energy using a PVDF transducer with an acrylic resin backing. *Measurement*. 2011, **44**(7), 1279–1283. ISSN 0263-2241.

[56] SOYAMA, Hitoshi, Hiroyuki KUMANO a Masumi SAKA. A new parameter to predict cavitation erosion. *http://resolver. caltech. edu/cav2001: sessionA3. 002*. 2001.

[57] SOYAMA, Hitoshi, Andrzej LICHTAROWICZ, Takahiro MOMMA a Edward J WILLIAMS. A new calibration method for dynamically loaded transducers and its application to cavitation impact measurement. *Journal of fluids engineering*. 1998, **120**(4), 712–718. ISSN 0098-2202.

[58] CARNELLI, Davide, Ayat KARIMI a Jean-Pierre FRANC. Evaluation of the hydrodynamic pressure of cavitation impacts from stress–strain analysis and geometry of individual pits. *Wear* [online]. 2012, **289**, 104–111. ISSN 0043-1648. Dostupné z: doi:https://doi.org/10.1016/j.wear.2012.04.009

[59] FORTES PATELLA, Regiane a Jean-Luc REBOUD. A New Approach to Evaluate the Cavitation Erosion Power. *Journal of Fluids Engineering* [online]. 1998, **120**(2), 335–344.

ISSN 0098-2202. Dostupné z: http://dx.doi.org/10.1115/1.2820653

[60] PATELLA, Regiane Fortes, Jean-Luc REBOUD a Antoine ARCHER. Cavitation damage measurement by 3D laser profilometry. *Wear*. 2000, **246**(1-2), 59–67. ISSN 0043-1648.

[61] MARQUES, Paulo Villani a Roseana DA EXALTAÇÃO TREVISAN. An SEM-Based Method for the Evaluation of the Cavitation Erosion Behavior of Materials. *Materials Characterization* [online]. 1998, **41**(5), 193–200. ISSN 1044-5803. Dostupné z: doi:https://doi.org/10.1016/S1044-5803(98)00038-2

[62] BACHERT, Bernd, Gerhard LUDWIG, Bernd STOFFEL a Sven BAUMGARTEN. Comparison of different methods for the evaluation of cavitation damaged surfaces. In: *ASME 2005 Fluids Engineering Division Summer Meeting*. B.m.: American Society of Mechanical Engineers, 2005, s. 553–560.

[63] FRANC, Jean-Pierre, Michel RIONDET, Ayat KARIMI a Georges L CHAHINE. Material and velocity effects on cavitation erosion pitting. *Wear*. 2012, **274**, 248–259. ISSN 0043-1648.

[64] TZANAKIS, Iakovos, D G ESKIN, Anastasios GEORGOULAS a D K FYTANIDIS. Incubation pit analysis and calculation of the hydrodynamic impact pressure from the implosion of an acoustic cavitation bubble. *Ultrasonics sonochemistry*. 2014, **21**(2), 866–878. ISSN 1350-4177.

[65] CARNELLI, Davide, Ayat KARIMI a Jean-Pierre FRANC. Application of spherical nanoindentation to determine the pressure of cavitation impacts from pitting tests. *Journal of Materials Research*. 2012, **27**(1), 91–99. ISSN 2044-5326.

APPENDIX A

Images obtained on an electron microscope at different resolutions.

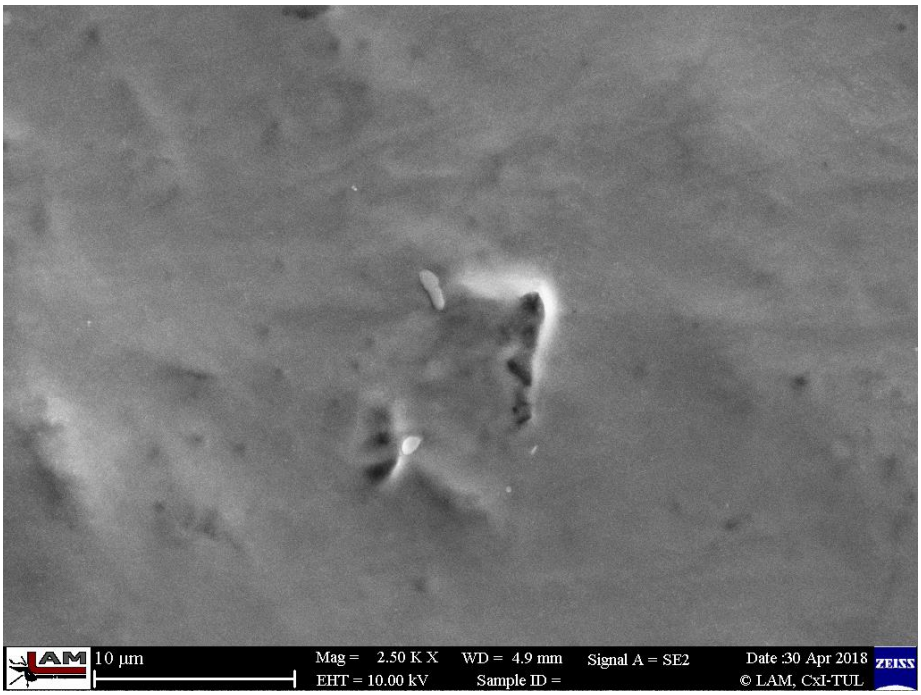

Figure 39: 2.50K X SEM micrograph (Sample 60 s) exposure to cavitation bubbles

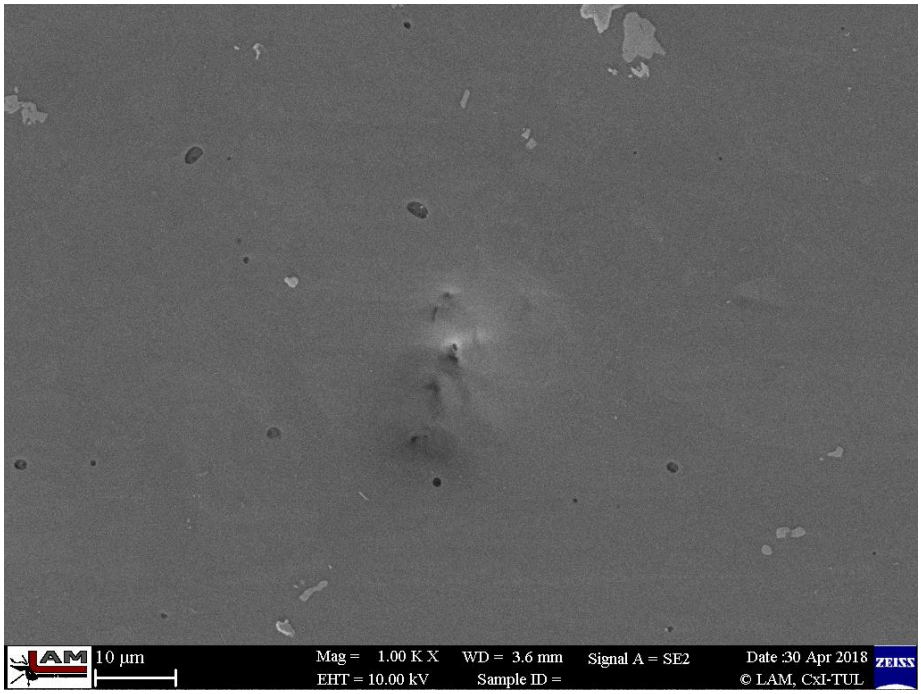

Figure 40: 1.00 K X SEM micrograph Sample 80 s exposure to cavitation bubbles